The role of the West Florida Shelf topography on the Loop Current system variability

Nektaria Ntaganou[1], Vassiliki Kourafalou[1], Matthieu Le Hénaff[2,3], and Yannis Androulidakis[1]

[1]University of Miami, Rosenstiel School of Marine and Atmospheric Science (RSMAS), Department of Ocean Sciences, Miami, FL 33149, USA

[2]University of Miami, Cooperative Institute for Marine and Atmospheric Studies (CIMAS), Miami, FL 33149, USA

[3]NOAA/Atlantic Oceanographic and Meteorological Laboratory (AOML), Miami, FL 33149, USA

Corresponding author:

Nektaria Ntaganou, email: nntaganou@rsmas.miami.edu,

ORCID: https://orcid.org/0000-0001-7027-2800

Conflict of interest: The authors have no conflict of interest.

For publication in

Ocean Dynamics

Abstract

The evolution of the Loop Current (LC) system under the interaction with the complex topography of the Gulf of Mexico (GoM) is examined. Focusing on the eastern GoM, we study the sole effects of the West Florida Shelf (WFS) topography on the LC system variability. We conduct numerical experiments using the free-running Hybrid Coordinate Ocean Model (HYCOM), at 1/25° horizontal resolution and 26 hybrid vertical layers. A simulation with realistic topography (*Control* run) has been performed over 8 years and we analyze the last 5-year period (2007-2011). Modified topography with a deeper and smoother continental shelf is then introduced and we perform a 5-year simulation over the same study period. In addition, we perform two independent experiments with the same topographic modifications that are initialized from fields during minimum and maximum LC northernmost extension. The results show that in the case of the modified shelf, the LC tends to extend farther into the GoM, with a predominant westward axis tilt, and rarely retracts south of 26°N even after Loop Current Eddy (LCE) shedding events. The results also suggest that although the LC can be in the vicinity of the southwestern tip of the modified WFS, it is not prevented from extending northward, as it usually happens in the simulation with realistic topography. Finally, the evolution of the LC into the GoM is influenced by lower layer processes associated with the bottom topography in the southwestern WFS and western Straits of Florida. More specifically, lower layer intensified/weakened positive potential vorticity signature promotes retracted/extended LC phases.

Keywords: West Florida shelf, HYCOM, mesoscale dynamics, topographic controls

1. Introduction

The Loop Current (LC) system, consisting of the LC and its associated eddies, governs the mesoscale circulation in the Gulf of Mexico (GoM) and is part of the Gulf Stream western boundary current. The LC flows into the GoM from the Yucatan Channel connecting the Caribbean Sea to the

GoM. Then, the LC exits the GoM through the Straits of Florida, where it feeds into the main Gulf Stream in the Atlantic Ocean. As the LC turns clockwise (anticyclonically) in the GoM, it generally flows along the West Florida Shelf (WFS), often approaching the shelf-break. The sole impact of the WFS topography on the LC evolution has not been studied in detail, although previous studies have concluded that it can be of great importance.

Weisberg and Liu (2017) found the intrusion of the LC into the GoM to be halted when it comes into contact with the southwestern tip of the WFS and suggested that the bottom topography of the region is an important factor controlling the penetration of the LC into the GoM. We aim to expand on those findings by isolating the topographic controls along the WFS and investigating their specific effect on the LC system. This is done with realistically forced, process oriented numerical experiments, by employing the Hybrid Coordinate Ocean Model (HYCOM; hycom.org; Bleck, 2002; Halliwell, 2004), applied in the Gulf of Mexico (GoM-HYCOM) at 1/25° horizontal resolution and 26 hybrid vertical layers. To address topographic controls, we perform topography experiments with modified WFS topography, which we compare to a *Control* run that simulates the dynamics of the area using the realistic GoM topography. As is appropriate for a process-oriented study, the simulations are free-running (no data assimilation).

As the LC flows through the GoM, it comes into contact with strong topographic gradients that can affect the evolution of the LC system (Chérubin et al., 2006; Oey, 2008; Le Hénaff et al., 2012). After shedding an anticyclonic eddy, the Loop Current Eddy (LCE), the LC may retract to the south, flowing directly from the Yucatan Channel to the Straits of Florida, also known as port-to-port configuration. A LCE usually goes through several detachments and reattachments to the main LC body prior to its final separation and westward propagation (Schmitz, 2005; Le Hénaff et al., 2012). In addition to the topographic gradients that the LC comes across, that are mostly located in the eastern GoM, topographic gradients in the western GoM also play a very important role in the circulation of the basin. In particular, Pérez-Brunius et al. (2018), based on observational data,

showed that interactions between eddies and the topography can influence the mean circulation of the deep western GoM.

Topographic controls also influence cyclonic eddies, known as Loop Current Frontal Eddies (LCFEs) that propagate around the LC. The LCFEs form upstream, usually along the Campeche Bank (Zavala-Hidalgo et al., 2003; Chérubin et al., 2006; Androulidakis et al., 2014; Le Hénaff et al., 2014; Garcia-Jove et al., 2016) and intensify as they flow over the Mississippi Fan region, which is located offshore of the Mississippi Delta (Le Hénaff et al., 2012; Garcia-Jove et al., 2016) and along the WFS (Oey, 2008). The generation of the LCFEs over the Campeche Bank can also be attributed to cyclonic vorticity inflow originating in the Caribbean Sea (Athié et al., 2012), combined with upwelling processes over the shelf of the Campeche Bank under prevailing easterly winds (Androulidakis et al., 2014). Garcia-Jove et al. (2016) showed the importance of the deep canyon of the eastern Campeche Bank on the intensification of the LCFEs, which are generated by instabilities in the LC. In their numerical topography experiments, the deep canyon of the eastern Campeche Bank was removed, showing that the LCFEs weakened and the LCEs were sparser. Previous studies have found that LCFEs play a role in the LCE shedding process (Le Hénaff et al. 2012; Donohue et al., 2016; Garcia-Jove et al., 2016). After the LCFEs reach the northern tip of the LC, they propagate southward affecting the curvature of the eastern side of the LC and, in some cases, they turn westward, promoting the "necking-down" phase of the LC, which leads to LCE formation (Schmitz, 2005; Le Hénaff et al., 2012). The process of the necking-down phase of the LC due to LCFEs was found to be facilitated by LCFE intensification governed by baroclinic instability along the WFS (Oey, 2008).

The role of the WFS topography on the LC evolution has been explored in previous studies. Hurlburt and Thompson (1980) conducted an extensive modified topography numerical study on the LC dynamics related to LC intrusion and LCE shedding. Using a non-linear two-layer model, forced solely by the inflow of water at the Yucatan Channel, with modified GoM bottom topography (depths ranging from 400m in the shelf regions to 3000m in the deepest part of the basin), they argued that

the topography of the WFS impacts the northward extension of the LC. More specifically, they showed that the LC is prevented from extending northward into the GoM, as a result of a local balance between advection and divergence in the southwestern WFS obtained from the continuity equation. Performing a different energetics analysis, Weisberg and Liu (2017) also investigated the penetration of the LC into the GoM, using satellite altimetry products from Archiving, Validation, and Interpretation of Satellite Oceanographic Data (AVISO) and the Self-Organizing Map technique to categorize the various LC behaviors in a number of patterns. After performing a heuristic volume control on the southwestern WFS region, they argued that the topography of the WFS can control the LC intrusion in the GoM. According to their study, for the LC to extend northward, it has to do work against buoyancy and bottom friction. In the case of a retracted LC, impinging on the southwestern tip of the WFS, the work required by the LC to extend northward is balanced by the work done by upwelling waters over the shelf and by bottom stress. This process, taking place on the southwestern tip of the WFS, which is located close to the steep topography surrounding Dry Tortugas (see Figure 1b) can halt the LC from extending northward into the GoM (Weisberg and Liu, 2017). In the case of the LC located away from the southwestern tip of the WFS, this balance no longer holds, and the LC can extend northward into the basin.

Hetland et al. (1999) also studied the results of the interaction between the LC and the WFS and concluded that when the LC impinges on the southwestern WFS, a strong southward jet is formed along the shelf break as a result of the pressure imposed by a retracted LC. Their argument was further consolidated by showing weak or no southward flow along the shelf break when the pressure was imposed on a broader shelf (i.e., north of the southwestern tip of the WFS). The findings were later confirmed by Weisberg and He (2003), who investigated the importance of local and deep-ocean forcing to the shelf water properties. They argued that the proximity of the LC to the Dry Tortugas, located at the southwestern WFS, promotes a southward jet along the entire shelf break that results in upwelling waters in the northern WFS (DeSoto Canyon) and upwelling at the southwestern tip of

WFS (Dry Tortugas), in agreement with Kourafalou et al. (2018). Recent observational and modeling findings also show that prolonged periods of the LC impinging on the southwestern WFS facilitate upwelling of cold waters over the Pulley Ridge (Figure 1b) and southern Dry Tortugas coral reefs by weakening the stratification of the WFS (Kourafalou et al., 2018).

The main goal of this study is to investigate the sole effects of the topography of the WFS, and especially the western slope of the WFS, on the LC system evolution. What distinguishes this study from the previous studies, on which we aim to expand on, is that we use a realistically forced, basin-wide model and we isolate the specific topographic effects of the WFS slope on the LC. We will discuss the dynamics of the LC and associated eddies under a modified WFS slope topography, with respect to the LC characteristics, such as the northward intrusion and LCE shedding. Focusing on events that exhibit significant differences between the *Control* and modified topography simulations, we explore the triggering mechanisms of the LC system variability associated with the WFS slope topography.

The model configuration and the methodology for the topographic modifications are presented in Section 2, followed by the LC spatial and temporal evolution in Section 3. The results, in terms of energetics and dynamical analysis are discussed in Section 4, and a brief concluding summary is provided in Section 5.

2. Model and Methodology

2.1 Model description

We employ the Hybrid Coordinate Ocean Model (HYCOM), which is a primitive equation ocean model with a hybrid vertical coordinate system. The configuration of HYCOM used in this study is applied in the GoM (GoM-HYCOM 1/25), at 3.8 km horizontal resolution (1/25°), with 26 hybrid vertical layers. Depending on the region of the ocean, the vertical coordinates are optimized to best represent the ocean dynamics of the area. The distribution is isobaric in the mixed layer, terrain-

following at the continental shelf, and isopycnal in the stratified ocean interior (Bleck, 2002). The model configuration is the same one used in Le Hénaff et al. (2012) and also performed without data assimilation. Their simulation was a 5-year free run from 2004 to 2008. Herein, we extended the run up to 2011. As described in Le Hénaff et al. (2012), the model was initialized using a 1-year long free running test simulation which was conducted at the Naval Research Laboratory (NRL) and the atmospheric forcing was derived from the Coupled Ocean Atmosphere Mesoscale Prediction System (COAMPS). The large-scale boundary conditions are described in Kourafalou et al. (2009), and the freshwater sources are treated as in Schiller and Kourafalou (2010).

The GoM-HYCOM 1/25 implementation was extensively validated against altimetry and *in situ* data by Le Hénaff et al. (2012); the model behavior was in good agreement with both remote sensing and *in situ* observations. The evaluation showed realistic LC variability, and standard deviation of extension and LC length. The Yucatan Current and LCE vertical structure comparisons with data were also in good agreement. Finally, the model could successfully resolve baroclinic instabilities, having simulated a first Rossby radius of deformation that matched the observational values in the GoM (20-30km).

2.2 Methodology – Topography experiments

The domain of GoM-HYCOM 1/25 covers the entire GoM, the Caribbean Sea north of 18°N and west of 76.4°W, and the Straits of Florida (Figure 1a). To address the topographic controls of the shelf, we introduce a modified WFS slope topography (Figure 1c), while the rest of the GoM topography remains the same, as shown in Figure 1a. This is the only difference in model parameters between the *Control* run (Figure 1b) and the modified topography experiments (Figure 1c). The modified topography is up to 200 m deeper than the realistic one, with the largest differences occurring near the shelf-break, between the 100-m and 500-m isobaths of the realistic topography. The purpose of this modification was to introduce not only a deeper, but also a smoother continental

shelf, based on a hypothesis that the interactions between LC system and the shelf slope would be more pronounced in deeper waters than in the surface. The 25- and 50-m isobaths are pushed eastward, with only the 50-m isobath now wrapping around the Dry Tortugas region, resulting in a deeper and smoother shelf (Figure 1c). The differences in topography are shown in Figure 1d and a vertical transect of the two topographies at 25°N is shown in Figure 1e. Hurlburt and Thompson (1980), in their idealized study, showed that the LC was unconstrained to extend northward when the idealized Florida Shelf was moved eastward. In our study, under the deeper and smoother WFS topography, we aim to investigate the behavior and variability of the LC system maintaining the relatively realistic character of the simulation.

By deepening the shelf and shelf break, we "create" a new volume of sea water. We simply extended horizontally the vertical structure found in the point neighboring the WFS at the time of initialization. By doing so, the isopycnal levels in the new volume are flat, and thus do not generate any unrealistic currents. Examination of all experiments showed no evidence of undesirable perturbations that could have been introduced by the modified topography. Figure A2 in the Appendix shows that the 2-year and 5-year averages from the simulation with the perturbed topography are consistent, which confirms that the results studied in the 2-year long *Topo-minLC* are robust and not due to transient effects of the perturbations.

For this study, we used the last 5 years (2007-2011) of an 8-year continuous control simulation (*Control* run), from which we determined the minimum (24.5°N on October 15, 2008) and maximum (28.52°N on December 13, 2007) northern LC extensions to initialize two independent modified topography simulations ("*Topo-minLC*" and "*Topo-maxLC*" experiments). Both independent simulations were conducted for ~2 years using identical forcing and boundary conditions to the *Control* run. The purpose of the two initializations, at the minimum and maximum LC northern extension, is to cover a large range of LC locations in short independent simulations and avoid any possible biases in the results that could emerge from initializing at only one state. In addition, the

two different initializations allow for comparison between the *Control* and modified topography experiments as soon as they start to diverge, while covering two different LC states. Finally, to assess the results from a longer-term perspective, we performed a continuous 5-year simulation as for the *Control* run, but with the modified WFS topography ("*Modified" experiment*). The *Modified* experiment was initialized at the same state as the analysis period of the continuous *Control* run (starting May 2007), and the results are presented in the Appendix. We note that the *Control* run covers an 8-year continuous period (2004-2011) and we analyze the last 5-year period starting on May 2007; this allows a fully developed mesoscale system in the GoM. A summarized list of the numerical experiments is provided in Table 1.

Table 1: List of numerical simulations

Experiment	Initialization	Length of run	WFS Topography
Control	May 2007	5 yrs	realistic
Topo-minLC	Oct 2008 (min LC extension)	2 yrs	modified
Topo-maxLC	Dec 2007 (max LC extension)	2 yrs	modified
Modified	May 2007	5 yrs	modified

3. Results

3.1 Case Studies

In this section, we are focusing on the early stages of the simulations and especially on the periods when the modified topography experiments, *Topo-minLC* and *Topo-maxLC,* start showing significant differences compared to the *Control* run. Since all experiments are initiated in the same way, there is a time period before the simulations completely diverge. This early period is analyzed, to elucidate the processes that govern the deviations between the two modified topography experiments from the realistic case with respect to the study processes. The entire study periods

(2 years for each case) were also analyzed to provide more statistical comparisons between *Control* and the two idealized experiments.

Topo-minLC experiment

Topo-minLC was initiated when the LC northernmost extension was minimum, based on the 5-year *Control* run. We are employing characteristic daily Sea Surface height (SSH) maps to showcase LC variability. The *Control* and *Topo-minLC* exhibit very similar behavior during the first three months, revealing the first differences in late January 2009 (Figure 2a, 2b). Although both LCs are close to the southwestern corner of the WFS, the western side of the LC in the modified topography simulation is more extended in a northwestward direction, with two large cyclonic eddies on the western and northern sides of the LC (~86.5°W and ~85°W, respectively). In the *Control* run, one intensified cyclonic eddy is located north of the LC (~85°W), promoting the LC's retracted phase up to February 18, 2009 (Figure 2c). The LC in the *Topo-minLC*, gradually extends northward after February 18, 2009 (Figure 2d), with cyclonic eddies propagating around the LC until mid-March 2009 (Figure 2h). The LC in the modified topography simulation extends farther into the GoM later in spring of 2009 in contrast to the *Control* run making the direct spatial comparison between the two experiments more difficult (not shown). The LC in the *Control* run is tilted toward the east in almost all cases presented in Figure 2 (Panels 2a, 2c, 2e, 2g), characterized by a constant interaction with the shelf and a continuous retracted position.

Topo-maxLC experiment

Figure 3 presents the SSH spatial evolution of the system from January 10 to March 10, when a final LCE separation occurs, as simulated in the *Control* run. The LCE detachment in the *Control* run is facilitated by the presence of a cyclonic eddy on the eastern side of the LC on January 30 (Figure 3c). The same frontal eddy also evolves in the *Topo-maxLC* experiment (Figures 3d, 3f), but it only leads to a temporary detachment of the LCE (Figure 3h). The LCE in the *Topo-maxLC* undergoes

several detachments and reattachments and remains relatively extended (north of 26°N), even after the LCE detachment on August 7, 2008 (Figure 4b), similarly to the *Topo-minLC.*

3.2 Loop Current evolution during the modified topography and *Control* experiments

As identified in Section 3.1, the first and most striking difference between the modified topography and *Control* experiments is the LC northernmost extension (Figures 4a, 4b). The LC extension is calculated by tracking the northernmost extension of the 17-cm Sea Surface Height (SSH) anomaly contour in the GoM, as introduced by Leben (2005). The LC in the *Topo-minLC* experiment quickly extends farther into the GoM than the *Control* run and sheds 2 anticyclonic LCEs (dashed red lines; Figure 4a) during a 2-year period (mid-October to late December 2010). The LCEs in the *Topo-minLC* undergo many detachments and reattachments before their final separation from the main LC body. Despite this activity, the LC remains at a relatively extended phase, north of 26°N, even after the LCE final separations on July 25, 2009 and May 11, 2010 (Figure 4a). On the other hand, the LC in the *Control* run is less elongated almost during the entire 2-year period and finally sheds a LCE on August 4, 2010 (Figure 4a). The LC in the *Topo-maxLC* (Figure 4b), similarly to the LC simulated in the *Topo-minLC* experiment, after shedding a LCE (June 5, 2008), quickly goes back to an extended phase until the end of 2009. Conversely, the LC in the *Control* run retracts south of 25°N after the LCE final separation on February 27, 2008 and stays retracted until the end of 2008 (Figure 4b). In summary, the LCs in the modified topography experiments are less constrained in terms of northward extension.

Depending on its extension, the LC may exhibit an eastward or westward tilt. We define the tilt as the angle formed between the axis of the LC and the 21.5°N latitude line. The axis of the LC (Figure 1a) is defined based on Androulidakis et al. (2020) as the line that connects the westernmost point of the 17-cm SSH anomaly contour at 21.5°N (inside the Yucatan Channel), which represents the base of the LC, to the point of the northernmost latitude of the 17-cm SSH anomaly contour, which

represents the LC northern extension latitude. The position of the LC inside the Yucatan Channel is variable and may depend on the phase of the LC (retracted, extended, necking-down position; Mildner et al., 2013) or on Caribbean eddies (cyclonic at the west and anticyclonic at the east of the LC inside the Yucatan Channel) that propagate toward the Yucatan Channel and interact with the LC (Oey et al., 2003; Athié et al., 2012, Androulidakis et al. 2021a). Another factor that could indirectly influence the position of the LC axis is the topography of the Yucatan Channel and Campeche Bank, which has been shown to affect the generation and evolution of cyclonic LCFEs (Zavala-Hidalgo et al., 2003; Chérubin et al., 2006; Garcia-Jove et al., 2016). The interaction between the LC and the LCFEs that form at its west side could affect the axis orientation.

In the case of the *Topo-minLC*, when the LC is more elongated, the axis angles are generally smaller than the ones in the *Control* run (Figure 5a). In particular, the LC in the modified topography simulation shows a mean axis angle of 86.4° ± 13.6°, i.e. it has a slight westward tilt (<90°), whereas the tilt of the LC in the *Control* run has a mean axis angle of 101.7° ± 15.9°, i.e. an eastward tilt (>90°). In Figure 5b the differences between the *Topo-maxLC* and the *Control* run are more pronounced, since the LC in the *Topo-maxLC* quickly extends much farther into the GoM after the LCE final separation than in the *Control* run, showing large differences in the northernmost extension (Figure 4b). The axis angles in the *Topo-maxLC* are generally acute, with a mean of 76.6°±12.5° corresponding to a westward tilt, whereas the LC in the *Control* run, which stays retracted for a long period of the run after the final LCE separation, exhibits a very pronounced eastward tilt with a mean angle of 108.9°±16.6° (Figure 5b).

Figures 6a and 6b show the relationship between the LC axis angle and northernmost extension in the *Control/Topo-minLC* and *Control/Topo-maxLC* experiments, respectively. This comparison suggests that the LC tilt is inversely proportional to the LC northern extension, with the larger angles associated to retracted LC phases. The *Topo-minLC* shows quite similar behavior to the *Control*, when the LC is located south of 26.5°N, but differences in the spread of the values are more

profound when the LC is north of 26.5°N (Figure 6a). The linear fits of the *Control*/*Topo-minLC* experiments are quite similar (slope is -13.25 for the *Control* and -10.14 for *Topo-minLC*). However, when the LC is extended north of 26.5°N, there is a wide range of axis angles, between 40° and 100°, which shows high variability of the LC axis tilt, suggesting that the LC of the *Topo-minLC* starts to diverge from the realistic case. The connection of the LC phases to the tilt of the LC axis, as well as the shift of the LC core, have been discussed by Hurlburt and Thompson (1980) and Athié et al. (2012). Hurlburt and Thompson (1980) associated eastward LC axis tilts with retracted LC phases and Athié et al. (2012) showed that the westward shift of the LC core preceded LCE shedding events. The shift of the LC core is easily connected to the shift of the LC axis angle following the definition of the axis angle in Figure 1a. Thus, high LC axis variability of acute axis angles, when the LC is extended, suggests a wide range of westward tilt positions that guarantee LCE shedding. On the other hand, high LC axis variability with angles larger than 90°, under an extended LC, is possibly connected to intensified LC curvature because of LCFE activity on its eastern side. In the case of the *Topo-maxLC*, the slope of the *Control* is -13.9 (Figure 6b), similar to the *Topo-minLC,* (Figure 6a). The LC system in the *Topo-maxLC* exhibits a quite different behavior with respect to the relationship between the LC northern extension and the LC axis angle. The variability of the axis angles for latitudes higher than 26.5°N in the *Topo-maxLC* agrees with *Topo-minLC* and the slope of the linear fit line is -3.9 (Figure 6b), less steep than the one in the *Control*. This indicates a larger deviation of the LC system in the *Topo-maxLC* simulation from the realistic case for the entire range of latitudes, not just the ones higher than 26.5°N. More specifically, for latitudes between 24.5°N and 26.5°N, the LC of the *Topo-maxLC* generally has a smaller axis tilt than the LC in the *Control*, indicating a predominant westward tilt during the entire simulation period. However, the data points at lower latitudes (south of 26.5°N) are far sparser, since the LC in the *Topo-maxLC* remained extended for almost the entire period (Figure 4b), making the *Topo-maxLC* less suitable for elucidating a clear relationship with the *Control* at latitudes south of 26.5°N.

Figures 6c and 6d show the percentage of axis angle occurrence for LC axis angles when the LC is at an extended phase (north of 26.5°N), for the *Topo-minLC* and *Topo-maxLC,* respectively. The modified topography experiments show a lager angle variability, with most ranges varying from 50° to 100°, whereas the *Control* exhibits a range of angles from 70° to 100°, when the LC is extended. When the LC is retracted or south of 26.5°N, the largest percentage of axis angles happens at 100° and 110° in the *Control* and 90° and 100° in the *Topo-minLC* (Figure 6e). This suggests that the LC in the *Control* exhibits more eastward tilt at its retracted phase and that the topography can also be a controlling factor of the LC variability when the LC is at lower latitudes. This is also shown in Figure 6f, for the period of the *Topo-maxLC* simulation. The LC in the *Topo-maxLC* exhibits axis angles mostly around 90° when it is retracted, with apparent low axis variability. However, fewer data points at this latitude range do not allow for a robust conclusion. Overall, the relationship between the LC northern extension and the axis tilt indicates a more unstable extended LC (north of 26.5°N), with higher axis variability in the modified topography simulations, in comparison to the realistic case (*Control* experiment).

Previous studies have connected the LC intrusion into the GoM to the proximity of the LC to the southwestern tip of the WFS (Hurlburt and Thompson, 1980; Hetland et al., 1999; Weisberg and Liu, 2017). According to these studies, the retracted LC phase usually coincides with the LC located very close or over the southwestern tip of the WFS. The study by Weisberg and Liu (2017) showed that a "pressure point" is created at the region close to Dry Tortugas (DT), characterized by steep topography (see Figure 1b for DT location). When the LC impinges on the vicinity of this region, pressure is imposed on the southwestern WFS and because of the strong topographic gradient, southward flow is exhibited along the entire WFS. Using a heuristic volume control, Weisberg and Liu (2017) argued that this "pressure point" can halt the LC from extending northward into the GoM. The "pressure point" is an important region with ecological implications as it is associated with the absence of *K. brevis* bloom conditions, when the LC impinges on the southwestern WFS for prolonged

time periods (Liu et al., 2016). Chiri et al. (2019) also confirmed the findings by Weisberg and Liu (2017), stating that when the LC extends northward into the GoM, its eastern part shifts westward and away from the vicinity of the southwestern WFS. Yang et al. (2020) found that the "pressure point" region is characterized by high values of pressure work that are associated with LCE shedding phases. In this study, we use our topography-modified numerical experiments to examine the influence of WFS slope topography on the LC evolution. We thus extend previous findings associated with the "pressure point" effects, but also offer a more general examination of the broader WFS slope region interactions with the LC.

Extending the findings by Weisberg and Liu (2017) about the effect of the "pressure point" on the LC evolution, we examine the proximity of the LC to the southwestern WFS. In the *Control* experiment (Figure 7a), the LC is initially retracted and as it extends northward, it also gradually moves west of the southward tip of the WFS at 24.2°N - 83.5°W. When the LC is extended, LCFEs propagate southward along its eastern side (i.e. Figures 3a, 3c), promoting the LC's intensified curvature that causes the rapid changes in the longitude of the 17-cm contour between October 11, 2009 and August 4, 2010 (Figure 7a). After the LCE final separation occurred on August 2, 2010 (Figure 7a, dashed blue line), after which the LC retracts to the south and moves about 25 km toward the shelf (east of 83.5°W). The topography of the southwestern WFS is not as steep in the *Topo-minLC* and, therefore, the process described above is not as clear because the aforementioned "pressure point" is disrupted. In the *Topo-minLC* experiment the LC is extended far into the GoM around mid-November 2009, but its eastern side is very close to the southwestern tip of the WFS (Figure 7b). This evolution suggests that the modified topography might not have the same effect on the LC northern extension and that the impact of the "pressure point" might no longer be as effective as it is in the realistic cases. However, there are periods when the LC is simultaneously extended and away from the shelf (April and August 2009, Figure 7b), supporting the process described by Weisberg and Liu (2017) and the *Control* run results, even under the modified topography. These brief periods are in

strong contrast to the much stronger connection of LC extension and the topographic controls around the realistic slope of the southwest WFS edge, which are supported by our results and previous studies. We also determined changes in the evolution of the cyclonic LCFEs that propagate between the eastern side of the LC and the WFS slope during extended LC phases, affecting the LC's curvature, as explained above. We found that these are connected to the rapid changes in the LC longitude at 24.2°N in the *Topo-minLC* (Figure 7b).

The LC in the *Control* spent more than 400 days east of 84°W (Figure 7c), exhibiting low variability regarding its position relatively to the southwestern tip of the WFS, which is attributed to the extended periods of retracted LC phases. On the other hand, the LC in the *Topo-minLC* spent around 300 days east of 84°W with higher occurrence frequencies at more western positions (>84°W; Figure 7d), showing larger variability regarding its proximity to the southwestern tip of the WFS. It is thus evident that the interaction of the LC with the southwestern WFS in the *Control,* is not as strong as in the *Topo-minLC,* when the LC is no longer anchored to the southwestern tip of the WFS.

After the LCE separation in the *Control* on February 27, 2008 (Figure 8a), the LC retracts to the south as it moves closer to the southwestern WFS, east of 83.5°W (Figure 8a), which is consistent with the "pressure point" theory. On the other hand, the LC starts to move away from the southwestern WFS (west of 83.5°W), after December 17, 2008. Since the LC is away from the vicinity of the southwestern WFS, it is implied that pressure is not anymore imposed by the LC on the "pressure point". In the *Topo-maxLC* experiment (Figure 8b), the abrupt changes in the longitude of the southeastern side of the extended LC make a clear relationship between the LC northern extension and proximity to the southwestern WFS difficult to determine. The LC is away from the shelf for almost the entire simulation period, with an exception at the end of the simulation period when the LC is extended both northward and eastward toward the shelf. The LC in the *Control* is mostly located east of 84°W for almost the entire study period (Figure 8c), since it quickly retracts to

the south after the LCE separation on February 27, 2008 (Figure 8a). Conversely, the proximity of the LC in the *Topo-maxLC* exhibits a wide range of values and as a result a larger variability (Figure8d) in agreement with the *Topo-minLC* variability (Figure 7d), which is also an indicator of reduced interaction between the LC and the southwestern tip of the WFS in the modified topography simulations.

Overall, the simulated LC in *Topo-minLC* and *Topo-maxLC* simulations exhibits a behavior that differs substantially from the *Control* run, with respect to its intrusion in the GoM, its axis tilt, and its proximity to the southwestern WFS. In the modified topography simulations, the LC maintains an extended phase, in contrast to the *Control* run (Figures 4a, 4b). This result is also supported by the long-term (5-year) continuous simulation, which is presented in the Appendix. The results do suggest that the LC in both modified topography simulations can be located close or away from the WFS, while maintaining a westward axis tilt and an extended phase (Figures 7b, 7d, 8b, 8d).

4. Discussion

4.1 Energetics analysis

The topographic controls are further examined to quantify their influence on the eddy dynamics of the GoM. Previous studies have shown an increase in Eddy Kinetic Energy (EKE) during LCE detachments/reattachments and before the LCE final separation events. Using a numerical model, Chérubin et al. (2006) computed EKE in a box that included the growing and shedding areas of the LC. Looking at six shedding cycles, they found an EKE increase before the LCE final separation events. Using observations, Donohue et al. (2016) calculated EKE in a very similar region as Chérubin et al. (2006), and showed that it increases before LCE shedding events.

Focusing on processes along the WFS and in the Straits of Florida, we computed EKE in two boxes (upper ~80 m; Figure 1a) that differ from the ones used in Chérubin et al. (2006) and Donohue

et al. (2016), who mostly focused on the growing areas of the LC located in the deep GoM. For the depth-integrated EKE we focus on the upper ~80m that represent the mixed layer, an approach that also differs from Donohue et al. (2016) who calculated EKE in two different depths. Box 1 includes part of the southwestern WFS and the northern Straits of Florida, and ranges from 23.5°N to 25°N and 84°W to 81°W, to include processes that take place in the vicinity of the "pressure point". Box 2 is located at the northwest of Box 1, and ranges from 25°N to 27°N and 86°W to 84°W to include processes that are related to cyclonic eddy activity, mostly LCFEs between the shelf and the LC. It also includes processes related to anticyclonic vorticity leakage from LC waters, when the LC impinges on the WFS (Zavala-Hidalgo et al., 2006; Kourafalou et al., 2018).

The EKE is calculated as follows:

$$EKE = \frac{u'^2 + v'^2}{2}, \quad (1)$$

where u' and v' represent perturbations from the mean state of the velocity field. We distinguish the mean state from the eddy field by passing a low pass Butterworth filter with a cutoff frequency of 1/60 days^{-1}, following Oey (2008) and Garcia-Jove et al. (2016). Thus, the low frequencies represent the mean state and changes related to the LC, while the high frequencies represent the mesoscale eddy field. In the *Control* run, there is high peak of EKE in each box before the final LCE separation, especially before the detachment on August 4, 2010 (Figures 9a and 9b) in agreement with Chérubin et al. (2006) and Donohue et al. (2016). The EKE in the *Control* run also reveals a smaller but profound increase during the LCE detachment in early 2008 in both boxes (Figures 10a and 10b). Such an increase is not evident in both modified topography experiments (Figures 9b and 10b). However, this is not a clear indication that the LCE separations are not associated with intensified cyclonic activity.

To elucidate whether the cyclonic activity east of the LC shifted from the area of Box 2 because of the very-well pronounced westward LC axis tilt (Figures 5a, 5b, red lines), we computed the EKE for the *Control* and *Topo-minLC,* before the LCE detachment events in both experiments for two

depth-averaged layers (Figures 9c-9f); the upper layer is the average of the EKE of model layers 1 to 15 and the mean EKE of the lower layer is the average of the EKE of model layers 16 to bottom, representing the mean upper and lower shelf ocean dynamics, respectively. Layer 15 (interface between the two averaged layers) is located at approximately 250 m and is isopycnal within the LC body and terrain-following at the continental shelf. The EKE increased in the upper layer of the *Control* right before the LCE detachment (July 29, 2010; Figure 9c), in agreement with the intensification exhibited in Box 2 (Figure 9b). Such intensification is not evident in any region east of the LC in the *Topo-minLC* (Figure 9d). The lower layer EKE shows similar behavior to the upper layer for both experiments, but with less pronounced intensification in the *Topo-minLC* compared to the *Control* (Figures 9e, 9f). In the lower layer of the *Control,* EKE is intensified mainly at the southeast of the LC (Figure 9e), evidence of the LCFE signature that is also pronounced in the upper layer (Figure 9c).

The region enclosed by Box 1 generally shows lower EKE values for the entire simulation period for both modified topography experiments, which suggests that the changes in topography have affected the eddy flow of the Box 1 region (Figures 9a and 10a). This implies that under a deeper and smoother topography the LCFEs generated in or transiting through the region enclosed by Box 1 are weakened. In the realistic case, as described by Hetland et al. (1999), there is intense southward flow when the LC is in the vicinity of the southwestern WFS. Kourafalou and Kang (2012) in their very high-resolution numerical modeling study, discussed the effects of topography of the Florida escarpment on local mesoscale and submesoscale cyclogenesis and found that the topography of the region plays a very important role in eddy growth, dissipation, and eddy-eddy interactions. They also noted that cyclonic eddy vorticity was fluctuating based on the eddy propagation over different depths. More specifically, the cyclonic vorticity increased when eddies propagated over deeper waters, whereas it decreased over shallower waters (process of vortex stretching). The presence of a southward flow in the region can facilitate cyclonic vortex formation due to the differences in the

topography as this flow enters the Straits of Florida, via the same process of vortex stretching discussed in Kourafalou and Kang (2012). When the southward flow, characterized by positive potential vorticity (i.e. Figure 11), reaches the southwestern WFS and enters the Straits of Florida, the positive potential vorticity would increase, assuming that it can be conserved locally and for short periods of time. In our modified topography experiments, due to the deepening of the topography, the process described above might not be as pronounced, resulting in weakened cyclonic activity in the area, even during periods of retracted LC in the vicinity of the southwestern WFS. However, this is not the only reason for cyclonic eddy presence in that region. Fratantoni et al. (1998) and Le Hénaff et al. (2014) have shown that the cyclonic eddies in the area are also transient or a result of merging between transient and locally formed eddies.

4.2 Dynamical Analysis

We examine the Potential Vorticity (PV) dynamics of the *Control* and modified topography experiments to further investigate the impact of the topographic controls of the WFS on the LC system evolution. Following Ertel's PV for a stratified fluid, PV is defined as:

$$q = (f\boldsymbol{z} + \boldsymbol{\nabla} \times \boldsymbol{u}) \cdot \nabla\left(-g\frac{\rho}{\rho_0}\right) = q_1 \cdot q_2 \quad (2)$$

where f is the Coriolis parameter, **z** is the unit vector of the z-coordinate, **u** is the velocity vector from which we take into consideration only the zonal and meridional components, g is the gravitational acceleration, ρ is the potential density, and ρ_0 is the reference density. The term q_1 represents the absolute vorticity, and q_2 represents the gradient of buoyancy. For our analysis, after calculating PV in every layer of the model, we divided the region in two layers. The PV in each of the two layers (upper layer: 1-15 model layers; lower layer: 16-26 model layers) was obtained by averaging in depth. As mentioned above, layer 15 of the model is chosen as the interface between the upper and lower layers, which can reach depth values of approximately 250 m in the deep GoM and 100 m in

the shelf region. Such separation of the water column allows for the investigation of upper and lower shelf interactions with the LC system.

Topo-minLC experiment

We seek to understand the processes related to the bottom topography of the WFS that contribute to the LC northern intrusion into the GoM, focusing on the periods early in the simulations when the two experiments (*Control* and *Topo-minLC*) start to significantly differ. Figure 11 shows the PV of the *Control* (left panels) and *Topo-minLC* (right panels) on February 14 and March 14, 2009, in both upper and lower layers. On February 14, the LC in the *Topo-minLC* is slightly more extended than the *Control* LC with cyclonic activity (positive PV) at the north of the LC in both simulations (Figures 11a and 11b). Although there is intensified signature of positive PV in the southwestern WFS and Straits of Florida that is evident in both experiments in the upper layer, the signature of positive PV in the lower layer in the *Topo-minLC* simulation (Figure 11d) is weaker than in the *Control* experiment (Figure 11c). The situation is quite similar in both experiments on March 14 when the positive PV signature of the lower layer in the *Topo-minLC* simulation (Figure 11h) is even weakened compared to the previous study case (February 14, Figure 11d). This coincides with the northern growth of the LC in the *Topo-minLC* experiment. As seen in Figure 4a, the growth rate of the northernmost extension of the LC is lower in the *Control* experiment, which appears to be associated with the presence of intensified positive PV in the lower layer over the southwestern WFS and Straits of Florida (Figures 11c and 11g).

Focusing on the term of the PV equation that corresponds to relative vorticity, we found that there is generation of positive vorticity from the interaction of the LC with the topography of the southwestern WFS in the *Control* that is not as evident in the *Topo-minLC* (Figures 12a-h). Starting from 24.5°N, positive vorticity, especially below 250 m, is generated when the LC is squeezed against the slope (Figures 12a and 12c), a signature that is also present at 25°N (Figures 12e and 12g).

Molemaker et al. (2015) and Gula et al. (2015) showed that the positive vorticity generation via the flow's interaction with topography is a process that can occur in the turbulent bottom boundary layer due to turbulent bottom stresses. Figures 12a, 12c, 12e, and 12g suggest that the LC in the *Control* might be related to that mechanism. According to Weisberg and Liu (2017), the LC northern intrusion is subjected to the work done by energy dissipation in the WFS and by buoyancy due to upwelling. If more energy is dissipated by bottom stresses, the work done by the LC will not be sufficient for the current to extend into the GoM.

When the WFS shelf and shelf slope are deepened in the modified experiments, the mechanism described above is not as easily facilitated (Figures 12b, 12d, 12f, and 12h). The positive vorticity is very weak along the slope (~83.5°W) on February 14, 2009 at both 24.5°N and 25°N (Figures 12b and 12f, respectively) and non-existent on March 14, 2009 at both 24.5°N and 25°N (Figures 12d and 12h, respectively). With the deepening of the slope, the interaction between the topography and the LC system has been reduced, which coincides with larger periods of extended LC phases in the *Topo-minLC* compared to the *Control.* If there is less interaction between the LC and the shelf slope, less energy could possibly be dissipated based on the mechanism described above and according to the findings by Weisberg and Liu (2017), there would be more energy available to the LC to penetrate the GoM. However, a more quantitative analysis is needed to confirm this hypothesis.

Further evidence that suggests a connection between positive PV in the southwestern WFS and the Straits of Florida with the LC northern extension and LCE shedding events is found during summers of 2009 and 2010 (Figure 13). Two characteristic dates represent the final LCE detachments in the *Topo-minLC* (June 14, 2009) and *Control* (August 4, 2010) experiments. On June 14, 2009 (Figure 13d), the LCE detachment in the *Topo-minLC* coincides with higher values of positive lower-layer PV in southwestern WFS and the Straits of Florida, compared to the PV values in the same region and layer on February 14 (Figure 11d) and March 14 (Figure 11h), 2009. The LCE detachment is also evident in the upper layer of the *Topo-minLC* (Figure 13b). Similarly, intensified lower layer

positive PV is present is the *Control* when the LC is retracted (Figure 13c) and during a LCE shedding event (Figure 13g). However, even though the increased lower layer PV in the southwestern WFS and Straits of Florida coincides with retracted LC phases and LCE shedding events in both numerical experiments, the lower layer PV signature in this region is not as intensified in the *Topo-minLC* even when the LC is similarly retracted (Figures 13c and 13d).

Since most of the differences between the two experiments occur in the southwestern WFS and the Straits of Florida, the lower layer positive PV of the *Topo-minLC* simulation is compared to the *Control* experiment in the area enclosed by Box 1 (Figure 14). In the *Control* experiment, the highest PV values are apparent when the LC is retracted, between May 3, 2009 and November 2009 as well as after the LCE detachment on August 4, 2010 (Figure 14a). These times periods coincide with LC extension latitudes south of 26°N, indicating that the LC is under a retracted phase. However, they drop quite abruptly when it enters its elongated phase and start increasing again after the LCE detachment. In the *Topo-minLC* simulation, the highest positive values happen when the LC is retracted (Figure 14a), or during LCE detachments, but they are lower than the positive PV values of the *Control* (Figure 14b). In both realistic and modified topography experiments, we see that intensified cyclonic activity, possibly connected to the mechanism described by Molemaker et al. (2015) and Gula et al. (2015), promotes a retracted LC phase, with either the LC remaining retracted or transiting to a retracted phase by shedding a LCE. However, in the *Topo-minLC*, since the positive PV signature is weaker because of the topographic modifications, the LC either remains extended for a prolonged period or very quickly returns to an extended phase a LCE shedding.

Because of the strong topographic gradient in the southwestern WFS region, if pressure is imposed on the isobaths that are located close to each other, the resulting flow along these isobaths will be present on the entire shelf as well. The southward jet, evident along the entire WFS when the LC impinges on the southwestern WFS (Hetland et al., 1999; Weisberg and Liu, 2017), is directly connected to the upwelling along the entire WFS. This process plays a role to the anchoring of the LC

in the southwestern corner of the WFS. According to Weisberg and Liu (2017), the work done by upwelling in the WFS is one of the factors that, if large enough, can halt the LC from extending northward into the GoM. The upwelling of deeper and colder waters is evident in both vertical sections in the *Control* from the steep slopes of the 10°C isotherm at 84°W (Figures 12a and 12c) and at 84°W (Figures 12e and 12g), indicating the presence of cold waters being pushed against the shelf slope when the LC is in the vicinity of the pressure point (Figures 12a, 12e). This is not as pronounced in the *Topo-minLC,* in which the 10°C isotherm has a less steep zonal gradient adjacent to the shelf slope (Figures 12d, 12f, and 12h).

We now examine the southward jet in the early days of the simulation (Oct 29 – Nov 29, 2008), when the LC in the *Control* was retracted and in the vicinity of the southwestern WFS and its northward extension did not significantly differ from the LC derived from the *Topo-minLC*. The horizontally integrated southward currents along 27°N (Figure 1b) averaged over depth for the *Control* and *Topo-minLC* experiments for both the upper and lower layers are shown in Figures 15a and 15b, respectively. The upper layer southward flow is very similar in both cases in terms of both variability and magnitude, with the mean values also not exhibiting large differences (Figure 15a). The differences are more pronounced in the lower layer; the southward flow computed for the *Topo-minLC* is weakened, compared to the *Control* run, which is characterized by larger variability (Figure 15b). This also supports the above findings based on the PV analysis of the flow, which showed that the interactions of the LC system with the topography of the WFS are mainly evident in the lower layer.

Topo-maxLC experiment

The PV of the upper and lower layers for both *Control* and *Topo-maxLC* experiments was computed during the LCE final separation in the *Control* experiment (Figure 16). *Topo-maxLC* was initiated on December 13, 2007 and the results from the two experiments are quite similar up to mid-

February 2008 (not shown). However, a LCE separates from the main LC body in the *Control* run by the end of February (Figures 16a, 16c and Figure 4b), undergoing several detachments and reattachments before its final separation late July 2008 in the *Topo-maxLC* experiment (Figure 4b). Based on the hypothesis described above on the connection between the intensified positive PV along the southwestern WFS and the LC retraction to the south and LCE shedding, Figures 16c and 16d suggest that this hypothesis stands even under an extended LC. In the *Control* experiment, intensified positive PV in the lower layer west of 84°W (marking the southwestern corner of the WFS and the entrance of the Straits of Florida) coincides with the LCE shedding and southward retraction of the LC (Figure 16c). On the other hand, in the *Topo-maxLC* experiment, where the PV values in the same area are lower, the LC remains extended (Figure 16d).

The effects of topography on the lower layer PV at the entrance of the Straits of Florida, associated with the LC extension, are shown in Figure 17b for the 2-year period of the *Topo-maxLC* and *Control* experiments. The lower layer positive PV of the *Topo-maxLC* simulation exhibits lower variability and generally lower values compared to the *Control* run, with high values coinciding with the LCE detachments/reattachments and final separation (Figure 17a). In the *Control* run, although the same pattern is followed, the positive PV variability and values are higher, associated with the shallower WFS topography and the steeper slope in the southwestern WFS.

In summary, the modified topography contributed to the weakening of the positive PV values and variability of the lower layer in the southwestern WFS. This result is associated with the deepening of the shelf, which causes less interaction between the LC system and the shelf slope. Even though the focus of this study was mostly process- and case-oriented, the long-term effects of the WFS topography on the LC system are the same, as presented in the Appendix.

5. Conclusions

We investigated the role of the West Florida Shelf (WFS) topography in the LC system evolution, by conducting modified topography experiments with a deeper and smoother WFS slope. The results from these idealized experiments were compared to a *Control* experiment, representing the realistic topography. All numerical simulations were realistically forced (i.e. atmospheric and boundary conditions) covering the entire GoM region. Two targeted modified topography experiments were initialized at the minimum (*Topo-minLC*) and maximum (*Topo-maxLC*) latitude of the LC extension that occurred during the entire period of the multi-year realistic *Control* run. Overall, under a deeper and smoother WFS topography (modified experiments), the LC extends farther into the GoM regardless of its initial phase (retracted or elongated). The LC remains north of 26°N even after a LCE final separation and regardless of being initially retracted to the south or having reached its maximum northern latitude. The only exceptions occur for very short periods of time (less than a few days) during the LCE detachments; the LC finally returns to an extended phase after the separation events. This leads to the conclusion that the topography of the WFS is one of the controlling factors of the LC extension and hence plays a role in the variability of the mesoscale GoM circulation.

The prolonged periods of extended LC promote its westward tilt, characterized by small axis angles that are more frequent in the modified topography experiments than in the *Control* run. The studies by Hetland et al. (1999) and Weisberg and Liu (2017) suggested that when the LC is retracted, it usually comes to contact with the vicinity of the southwestern WFS (large axis angles). On the contrary, when it loses contact with the shelf, it is free to extend northward. We extended these previous findings by showing that even small changes in the topography of the southwestern WFS can lead to a simulated LC that is unconstrained to extend northward even when it contacts the modified shelf. We conclude that the unique topography of the southwestern WFS edge is an important factor in the LC evolution.

The results also showed that there is weaker lower layer cyclonic activity in the region of the southwestern WFS and the Straits of Florida in the *Topo-minLC* and *Topo-maxLC* experiments, as a consequence of the modified topography. Calculation of Eddy Kinetic Energy (EKE) in the southwestern WFS/Straits of Florida, as well as in the central WFS, shows increased cyclonic eddy activity associated with LCE shedding in the *Control* run, whereas no such increase was evident in the modified topography experiments. This suggests a connection of WFS topographic controls to LCE shedding.

Finally, our findings suggest that the increased interaction between the LC and the slope of the southwestern WFS can possibly contribute to the work done by bottom stresses and upwelling, through the generation of positive Potential Vorticity (PV), as described in Molemaker et al. (2015). This is also related to LC variability, as increased work done by bottom stresses and upwelling at the southwestern WFS can halt the LC from extending northward (Weisberg and Liu, 2017). However, there is need for future work for this hypothesis to be quantitatively confirmed. The mechanisms of the injection of PV at the bottom boundary layer could be evaluated in future studies using higher resolution numerical simulations to fully resolve submesoscale processes. After investigating the differences in PV between the *Control* and *Topo-minLC*/maxLC experiments, we conclude that the LC intrusion into the GoM is influenced, among other factors, by lower layer processes that take place in the southwestern WFS and Straits of Florida, connected to the topography (steepness and depth) of the region. These topographic controls were shown to influence the LC northernmost extension and, as a result, the LCE shedding. This was done by altering the lower layer southward flow over the WFS, as well as the positive vorticity generation when the LC contacts the southwestern WFS, and as a result, the variability of the positive lower-layer PV associated with the topography of this region.

The LC evolution is a complex process influenced by various other processes that take place both in a) the GoM such as LCFEs effects (Schmitz, 2005; Chérubin et al., 2006; Le Hénaff et al., 2012, 2014; Androulidakis et al., 2014), the LC meandering (Donohue et al., 2016), the momentum

imbalance paradox (Pichevin and Nof, 1997), mesoscale processes in the Straits of Florida (Androulidakis et al., 2021b), and b) in the neighboring Caribbean Sea, such as vorticity flux at the Yucatan Channel, wind conditions, and anticyclonic eddy presence upstream (Candela et al., 2002; Oey et al., 2003; Androulidakis et al.; 2021a). The topography of the WFS is one of the controlling factors of the LC intrusion in the GoM and future work is needed to characterize it in more detail.

Acknowledgments

This research was made possible by a grant from the National Academy of Sciences, Engineering and Medicine (Gulf Research Program UGOS #2000011056). M. Le Hénaff received partial support for work on this publication by NOAA/AOML and was supported in part under the auspices of the Cooperative Institute and Atmospheric Studies (CIMAS), a cooperative institute of the University of Miami and NOAA (agreement NA10OAR4320143).

Data Availability Statement

The datasets generated during and/or analysed during the current study are available from the corresponding author upon reasonable request.

References

Androulidakis, Y. S., Kourafalou, V. H., & Le Hénaff, M. (2014). Influence of frontal cyclone evolution on the 2009 (Ekman) and 2010 (Franklin) Loop Current eddy detachment events. *Ocean Science*, *10*(6), 947-965. https://doi.org/10.5194/os-10-947-2014

Androulidakis, Y., Kourafalou, V., Le Hénaff, M. *et al.* (2020). Gulf Stream evolution through the Straits of Florida: the role of eddies and upwelling near Cuba. *Ocean Dynamics* **70,** 1005–1032. https://doi.org/10.1007/s10236-020-01381-5

Androulidakis, Y., Kourafalou, V., Olascoaga, M.J., Beron-Vera, F.J., Le Hénaff, M., Kang, H., Ntaganou, N. (2021a). Impact of Caribbean Anticyclones on Loop Current variability, *Ocean Dynamics,* pp.1-22.

Androulidakis, Y., Kourafalou, V., Le Hénaff, M., Kang, H., & Ntaganou, N. (2021b). The Role of Mesoscale Dynamics over Northwestern Cuba in the Loop Current Evolution in 2010, during the Deepwater Horizon Incident. Journal of Marine Science and Engineering, 9(2), 188

Athié, G., Candela, J., Ochoa, J., and Sheinbaum, J. (2012), Impact of Caribbean cyclones on the detachment of Loop Current anticyclones, *J. Geophys. Res.*, 117, C03018, https://doi.org/10.1029/2011JC007090.

Bleck, R. (2002). An oceanic general circulation model framed in hybrid isopycnic-Cartesian coordinates. Ocean Modelling. 4. 55-88. 10.1016/S1463-5003(01)00012-9.

Candela, J., Sheinbaum, J., Ochoa, J., Badan, A., Leben, R., (2002). The potential vorticity flux through the Yucatan Channel and the Loop Current in the Gulf of Mexico. Geophys. Res. Lett. 29, 16-1-16–4.

Chérubin, L. Morel M., Y., and Chassignet, E. P. (2006). Loop Current Ring Shedding: The Formation of Cyclones and the Effect of Topography. *J. Phys. Oceanogr.*, **36**, 569-591, https://doi.org/10.1175/JPO2871.1.

Chiri, H., Abascal, A.J., Castanedo, S., Antolínez, J.A.A., Liu, Y., Weisberg, R.H., Medina, R., (2019). Statistical simulation of ocean current patterns using autoregressive logistic regression models: A case study in the Gulf of Mexico. Ocean Model. 136, 1–12.Donohue, K.A., Watts, D.R., Hamilton, P., Leben, R., and Kennelly, M. (2016). Loop Current Eddy Formation and Baroclinic Instability. Dynamics of Atmospheres and Oceans. 76. https://doi.org/10.1016/j.dynatmoce.2016.01.004.

Fratantoni, P. S., Lee, T. N., Podesta, G. P., and Muller-Karger, F. (1998). The influence of Loop Current perturbations on the formation and evolution of Tortugas eddies in the southern Straits of Florida, *J. Geophys. Res.*, 103(C11), 24759– 24779, doi:10.1029/98JC02147.

Garcia-Jove, M., Sheinbaum, J., & Jouanno, J. (2016). Sensitivity of Loop Current metrics and eddy detachments to different model configurations: The impact of topography and Caribbean perturbations. *Atmosfera, 29*, 235-265. https://doi.org/10.20937/ATM.2016.29.03.05

Gula, J., M. J. Molemaker, and J. C. McWilliams (2015). Topographic vorticity generation, submesoscale instability, and vortex street formation in the Gulf Stream, *Geophys. Res. Lett.,* 42, 4054-4062, doi:10.1002/2015GL063731.

Halliwell, G. (2004). Evaluation of vertical coordinate and vertical mixing algorithms in the HYbrid-Coordinate Ocean Model (HYCOM). Ocean Modelling. 7. 285-322. https://doi.org/10.1016/j.ocemod.2003.10.002.

Hetland, R. D., Hsueh, Y., Leben, R., & Niller, P. (1999). A Loop Current-induced jet along the edge of the West Florida shelf. Geophysical Research Letters, 26, 2239–2242. https://doi.org/10.1029/1999GL900463

Hurlburt, H. E., and Thompson, J. D. (1980). A Numerical Study of Loop Current Intrusions and Eddy Shedding. *J. Phys. Oceanogr.*, **10**, 1611–1651, https://doi.org/10.1175/1520-0485(1980)010<1611:ANSOLC>2.0.CO;2.

Kourafalou, V.H., Peng, G., Kang, H. *et al.* (2009). Evaluation of Global Ocean Data Assimilation Experiment products on South Florida nested simulations with the Hybrid Coordinate Ocean Model. *Ocean Dynamics* **59,** 47–66. https://doi.org/10.1007/s10236-008-0160-7

Kourafalou, V. H., and Kang, H. (2012). Florida Current meandering and evolution of cyclonic eddies along the Florida Keys Reef Tract: Are they interconnected?, *J. Geophys. Res.*, 117, C05028, doi:10.1029/2011JC007383.

Kourafalou, V.H., Androulidakis, Y.S., Kang, H., Smith, R.H., Valle-Levinson, A., (2018). Physical connectivity between Pulley Ridge and Dry Tortugas coral reefs under the influence of the Loop Current/Florida Current system. Prog. Oceanogr. 165, 75–99, https://doi.org/10.1016/j.pocean.2018.05.004

Le Hénaff, M., Kourafalou, V. H., Morel, Y., and Srinivasan, A. (2012). Simulating the dynamics and intensification of cyclonic Loop Current Frontal Eddies in the Gulf of Mexico, *J. Geophys. Res.*, 117, C02034, doi:10.1029/2011JC007279.

Le Hénaff, M., Kourafalou, V.H., Dussurget, R., and Lumpkin, R. (2014). Cyclonic activity in the eastern Gulf of Mexico: characterization from along-track altimetry and in situ drifter trajectories. Progress in Oceanography, 120:120-138. https://doi.org/10.1016/j.pocean.2013.08.002

Leben, R.R. (2013). Altimeter-Derived Loop Current Metrics. In Circulation in the Gulf of Mexico: Observations and Models (eds W. Sturges and A. Lugo-Fernandez). doi:10.1029/161GM15

Liu, Y., Weisberg, R. H., Lenes, J. M., Zheng, L., Hubbard, K., and Walsh, J. J. (2016). Offshore forcing on the "pressure point" of the West Florida Shelf: Anomalous upwelling and its influence on harmful algal blooms, J. Geophys. Res. Oceans, 121, 5501– 5515, doi:10.1002/2016JC011938.

Mildner, T. C., Eden, C., and Czeschel, L. (2013). Revisiting the relationship between Loop Current rings and Florida Current transport variability, *J. Geophys. Res. Oceans*, 118, 6648– 6657, doi:10.1002/2013JC009109.Molemaker, M.J., Mcwilliams, J.C., Dewar, W.K., (2015). Submesoscale instability and generation of mesoscale anticyclones near a separation of the California undercurrent. J. Phys. Oceanogr. 45, 613–629.

Oey, L.-Y., Lee, H.-C., and Schmitz, W. J. (2003). Effects of winds and Caribbean eddies on the frequency of Loop Current eddy shedding: A numerical model study, *J. Geophys. Res.*, 108, 3324, doi:10.1029/2002JC001698, C10.

Oey, L. (2008). Loop Current and Deep Eddies. *J. Phys. Oceanogr.*, **38**, 1426-1449, https://doi.org/10.1175/2007JPO3818.1.

Pérez-Brunius, P., Furey, H., Bower, A., Hamilton, P., Candela, J., García-Carrillo, P., and Leben, R. (2018). Dominant Circulation Patterns of the Deep Gulf of Mexico. *J. Phys. Oceanogr.*, **48**, 511–529, https://doi.org/10.1175/JPO-D-17-0140.1.

Pichevin, T., Nof, D. (1997). The momentum imbalance paradox. *Tellus*, **49 ,** 298–319.

Schiller, R. V., Kourafalou, V.H., (2010). Modeling river plume dynamics with the HYbrid Coordinate Ocean Model, Ocean Modelling 33 101–117, https://doi.org/10.1016/j.ocemod.2009.12.005

Schmitz, W.J., Jr. (2013). Cyclones and Westward Propagation in the Shedding of Anticyclonic Rings from the Loop Current. In Circulation in the Gulf of Mexico: Observations and Models (eds W. Sturges and A. Lugo-Fernandez). doi:10.1029/161GM18

Weisberg, R. H., and He, R. (2003). Local and deep-ocean forcing contributions to anomalous water properties on the West Florida Shelf, *J. Geophys. Res.*, 108, 3184, doi:10.1029/2002JC001407, C6.

Weisberg, R. H., and Liu, Y. (2017). On the Loop Current penetration into the Gulf of Mexico. Journal of Geophysical Research: Oceans, 122, 9679–9694. https://doi.org/10.1002/2017JC013330

Yang, Y., Weisberg, R.H., Liu, Y., Liang, X.S. (2020). Instabilities and multiscale interactions underlying the loop current eddy shedding in the gulf of mexico. J. Phys. Oceanogr. 50, 1289–1317.

Zavala-Hidalgo, J., Morey, S. L., and O'Brien, J. J. (2003). Cyclonic Eddies Northeast of the Campeche Bank from Altimetry Data. *J. Phys. Oceanogr.*, **33**, 623–629, https://doi.org/10.1175/1520-0485(2003)033<0623:CENOTC>2.0.CO;2.

Zavala-Hidalgo, J., Morey, S. L., O'Brien, J. J., & Zamudio, L. (2006). On the Loop Current eddy shedding variability. *Atmósfera*, *19*(1), 41-48. Recuperado en 20 de julio de 2021, de http://www.scielo.org.mx/scielo.php?script=sci_arttext&pid=S0187-62362006000100004&lng=es&tlng=en.

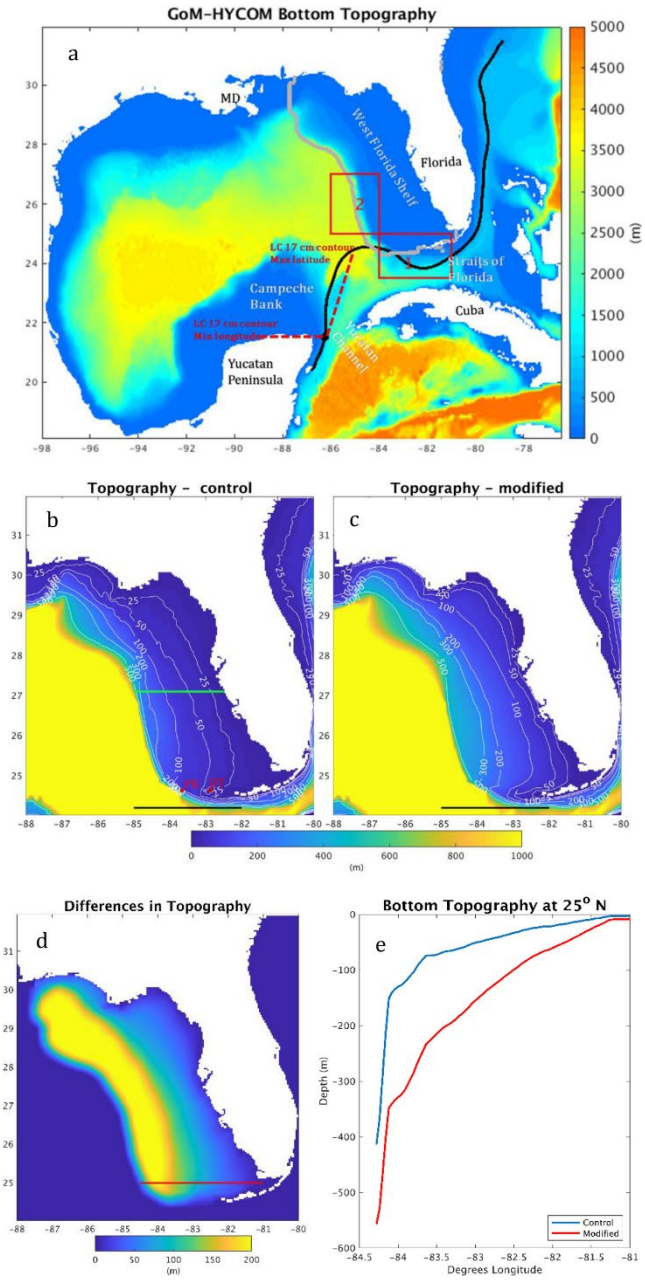

Figure 1: a) Gom-HYCOM bottom topography. The two boxes represent the regions where EKE is computed for both the *Control* and modified topography experiments. The dashed red lines represent the LC axis angle definition based on the position of the 17-cm Sea Surface Height (SSH) anomaly contour of the LC (solid black line). The gray line represents the boundaries of the WFS that were taken into account for the modifications of the bottom topography. The Mississippi Delta is marked as MD. b) Realistic WFS topography. The solid black line is drawn at 24.2°N, marking the southwestern tip of the WFS and is used for later calculations. The solid white lines represent the isobaths. The green line is drawn at 27°N, for later calculations. The red dot marks the location of Dry Tortugas (DT). c) Modified WFS topography. The solid white lines and the black line are the same as in b). d) Differences in topography of the WFS (realistic topography minus perturbed one). The solid red line marks the latitude where the transect for e) is shown. e) Bottom Topography transect at 25° N for the *Control* and modified topography experiments.

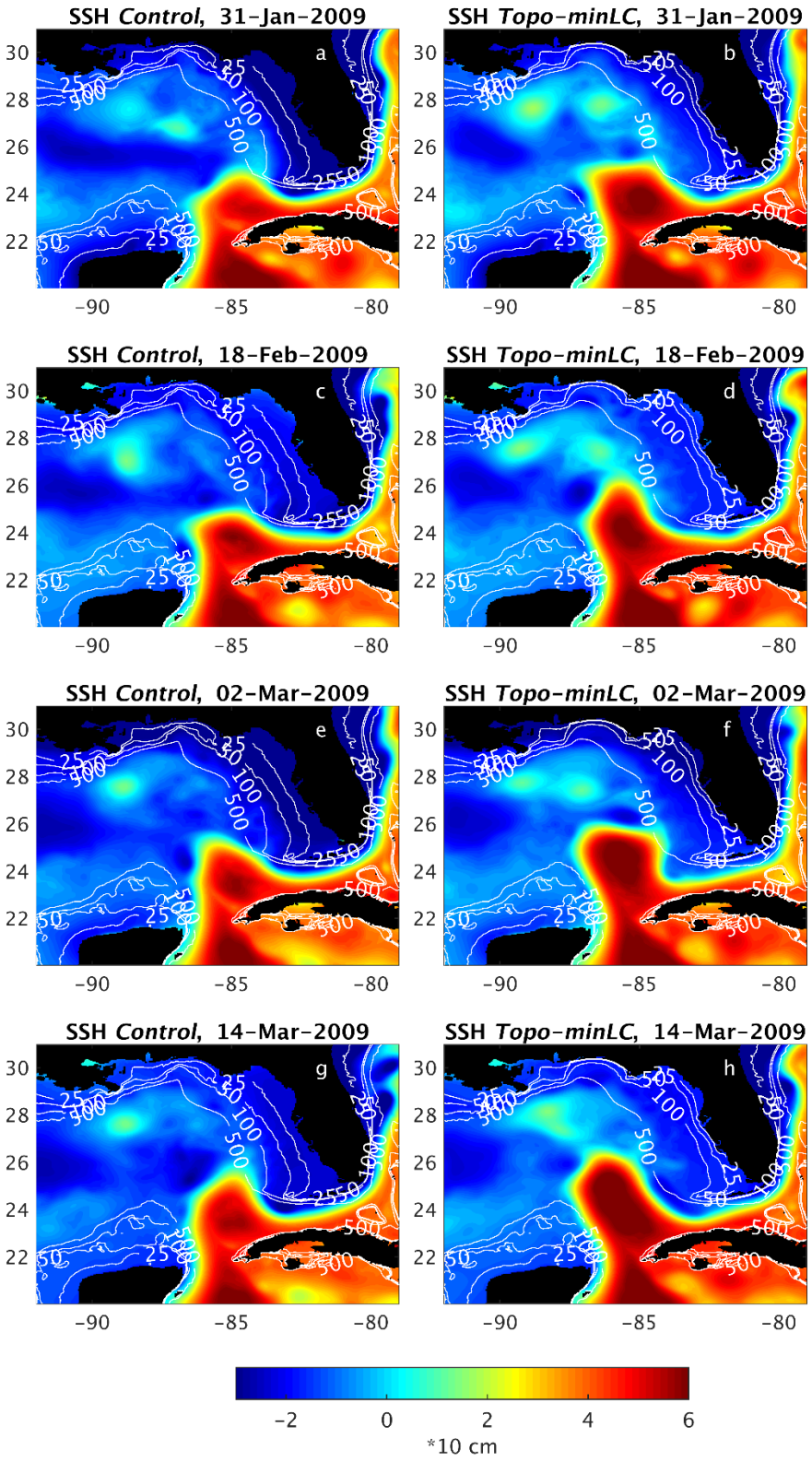

Figure 2: SSH for *Control* (left panels) and *Topo-minLC* (right panels) experiments, during January-March 2009. The solid white lines are the 25, 50, 100, and 500 m isobaths.

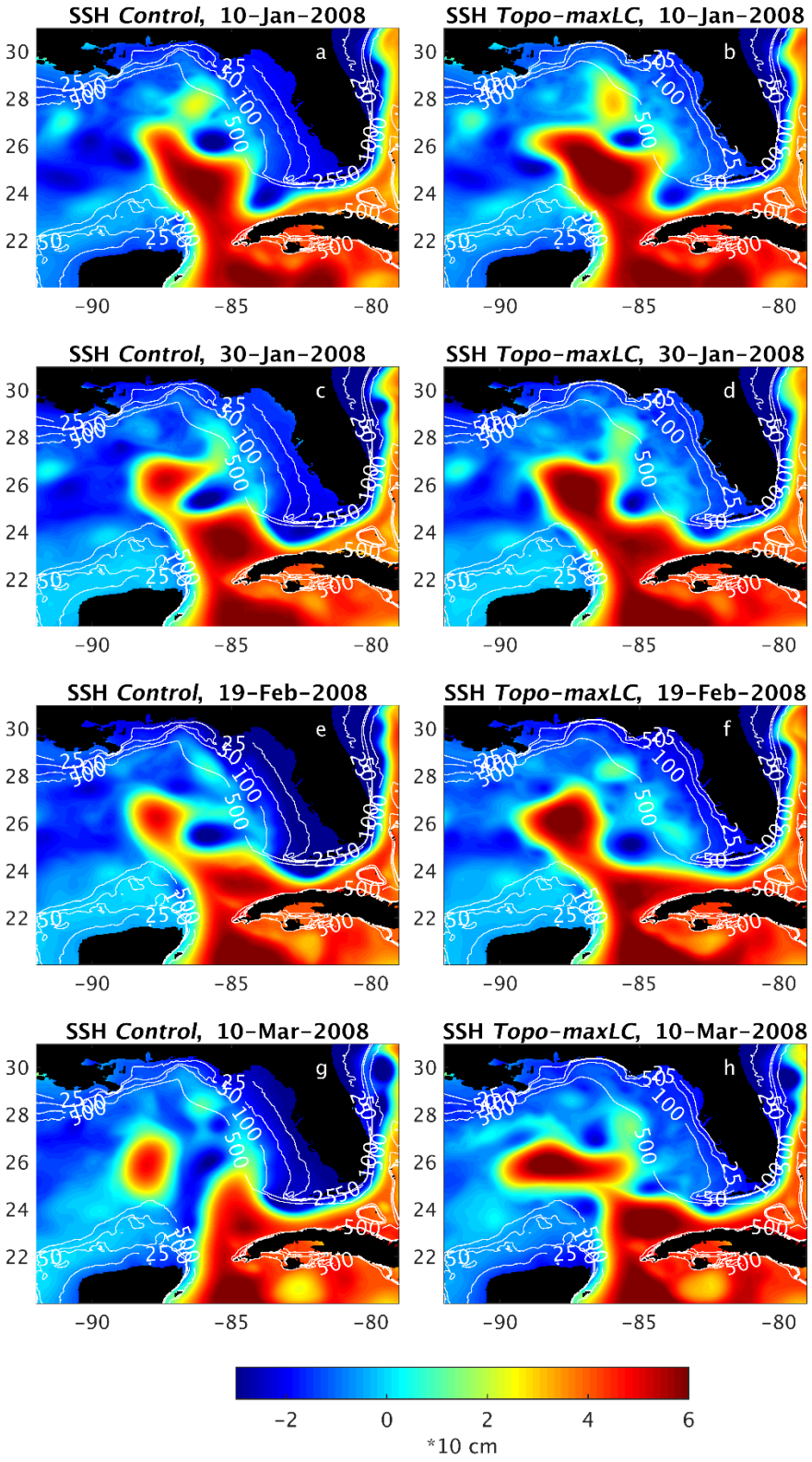

Figure 3: SSH for *Control* (left panels) and *Topo-maxLC* (right panels) experiments, during January-March 2009. The solid white lines are the 25, 50, 100, and 500 m isobaths.

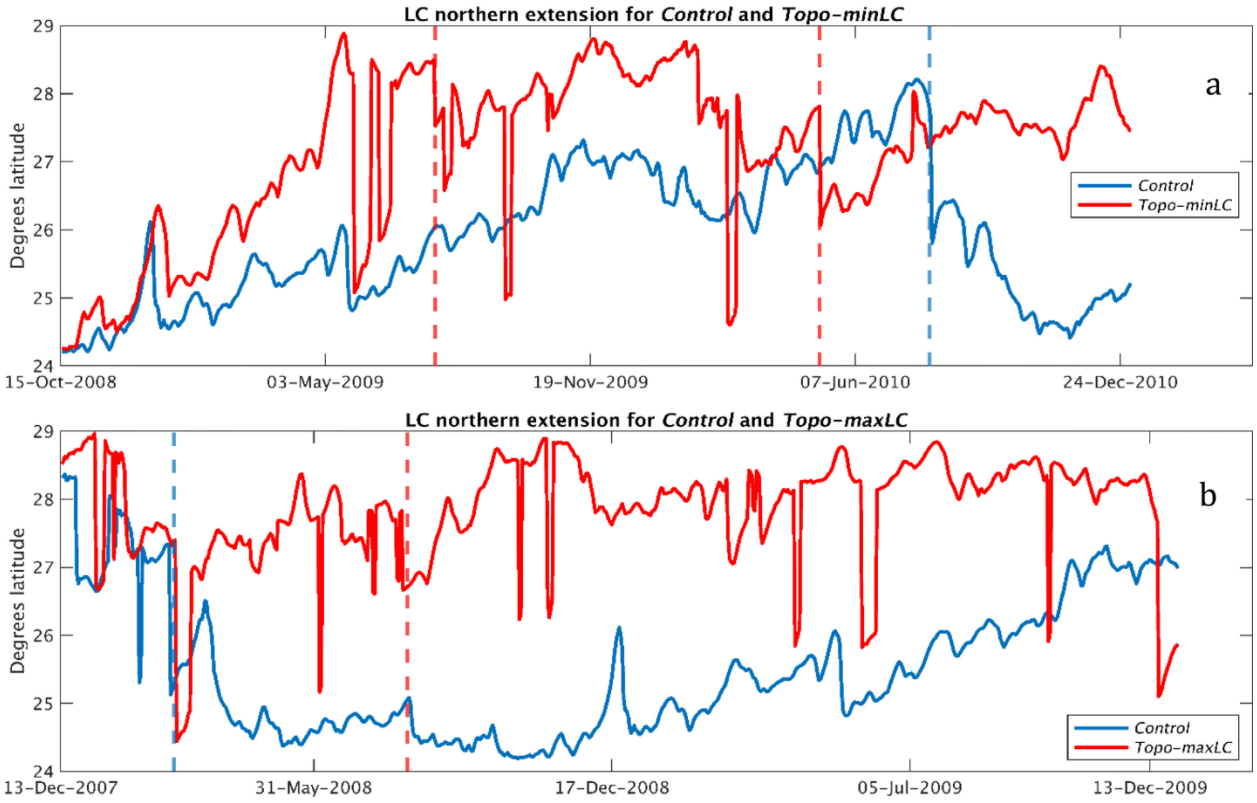

Figure 4: a) LC northernmost extension, based on the position of the 17-cm SSH anomaly contour for the *Control* (solid blue line) and *Topo-minLC* (solid red line). The dashed blue and dashed red lines represent the LCE final separations in the *Control* and *Topo-minLC* experiments. b) Similar to a), but with the red lines representing the *Topo-maxLC* experiment.

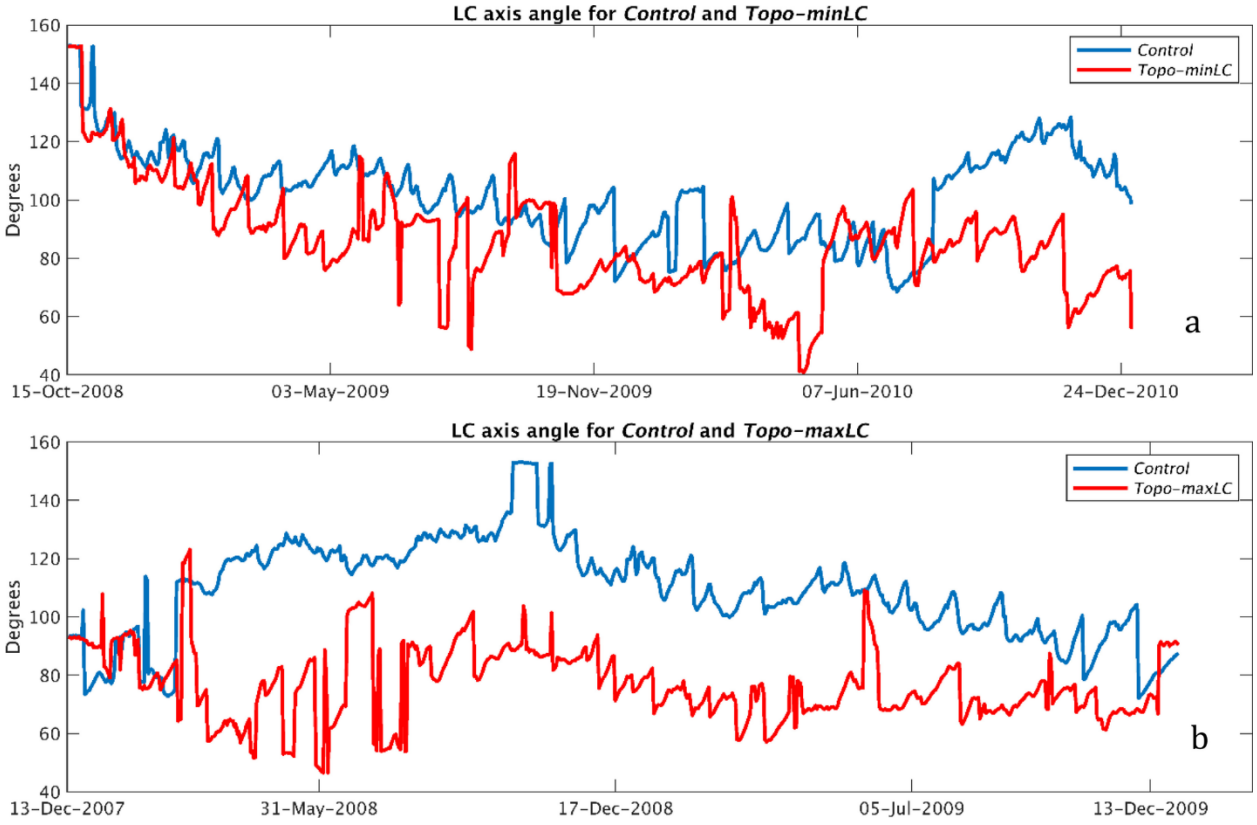

Figure 5: a) LC axis angle for the *Control* (solid blue line) and *Topo-minLC* (solid red line). b) Similar to a), but with the red line representing the *Topo-maxLC* experiment.

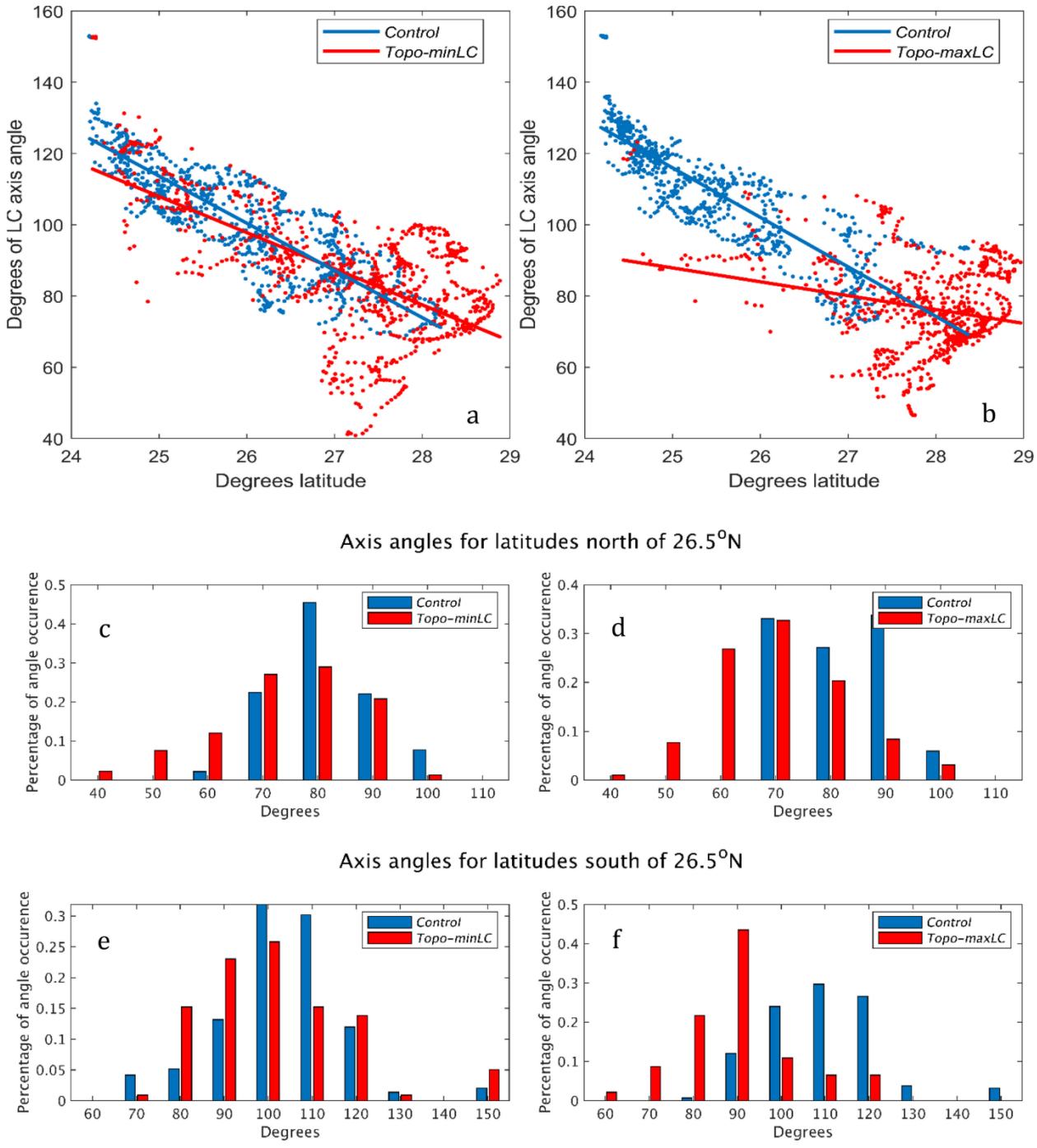

Figure 6: a) LC northernmost extension and LC axis angle for the *Control* and *Topo-minLC* experiments. The solid blue and red lines represent the linear fit for the *Control* and *Topo-minLC*, respectively. b) Same as a), but for the *Topo-maxLC.* c)-d) Percentage of axis angle occurrence for latitudes north of 26.5°N for *Control* and *Topo-minLC/Topo-maxLC,* respectively. e)-f) Same as c) and d), but for latitudes south of 26.5°N.

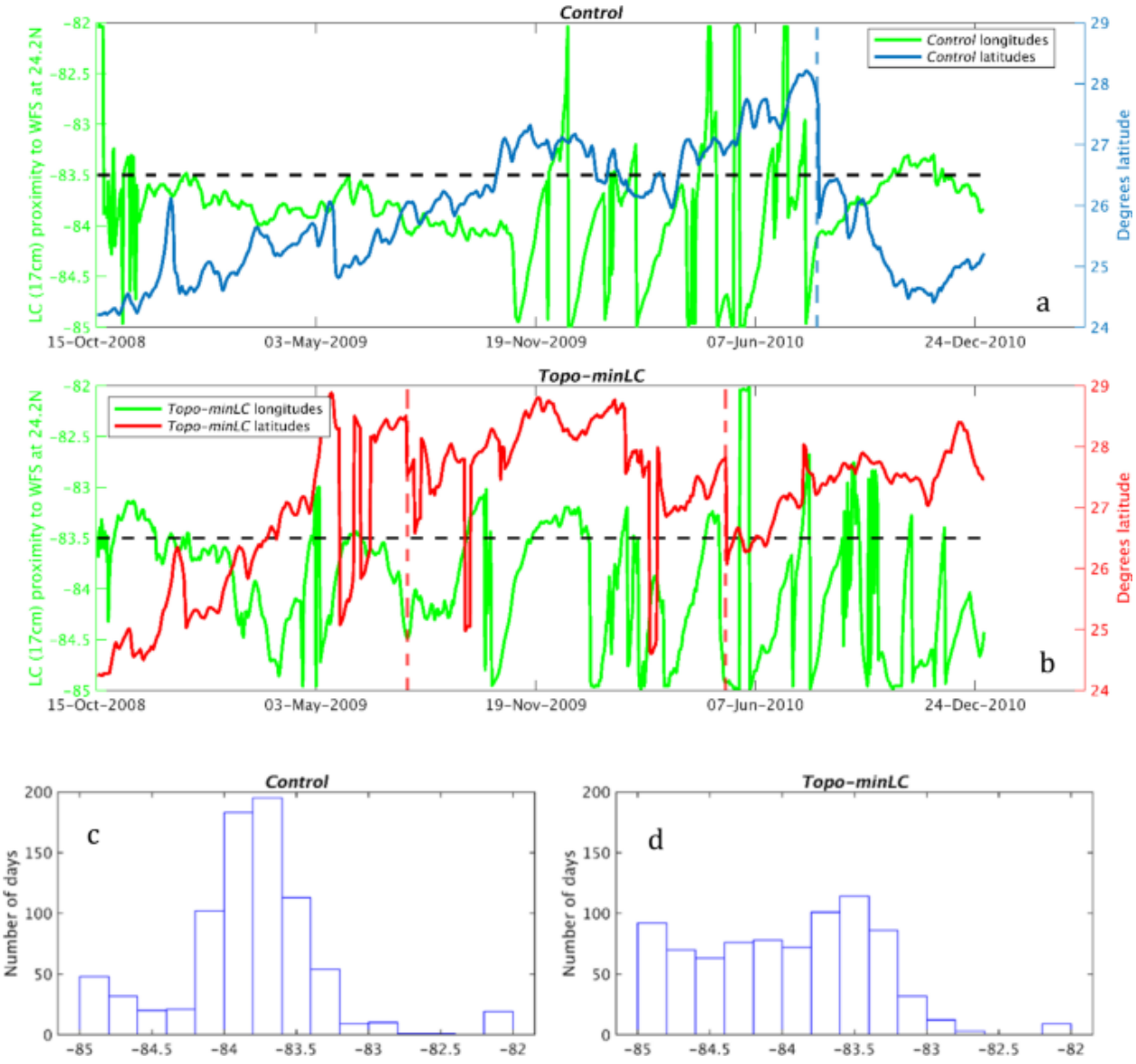

Figure 7: Easternmost longitude of the 17-cm SSH anomaly contour at 24.2° N as green lines for a) *Control* and b) *Topo-minLC* experiments; LC northernmost extension as a) blue line for *Control* and b) red line for *Topo-minLC* experiments; LCE final separations are marked with vertical dashed lines for a) the *Control* (blue dashed) and for b) the *Topo-minLC* (red dashed) experiments. The horizontal dashed black lines in a) and b) represent the longitude of the southwestern tip of the WFS at 83.5° W. c) Distribution of easternmost longitudes of the 17-cm SSH anomaly contour among the total period of the *Control* simulation. d) Same as c), but for the *Topo-minLC.*

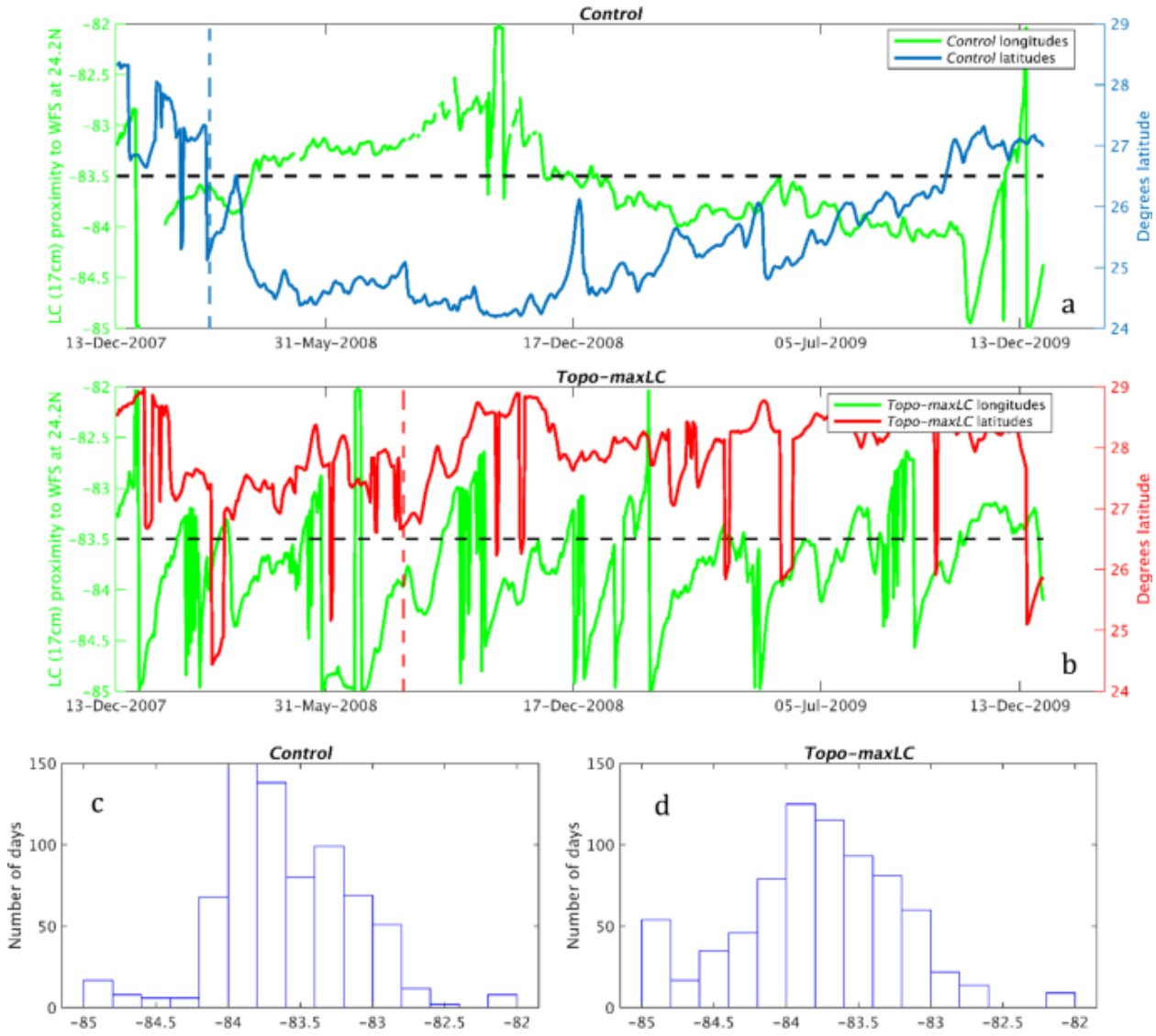

Figure 8: Same as Figure 7, but for the *Topo-maxLC* experiment.

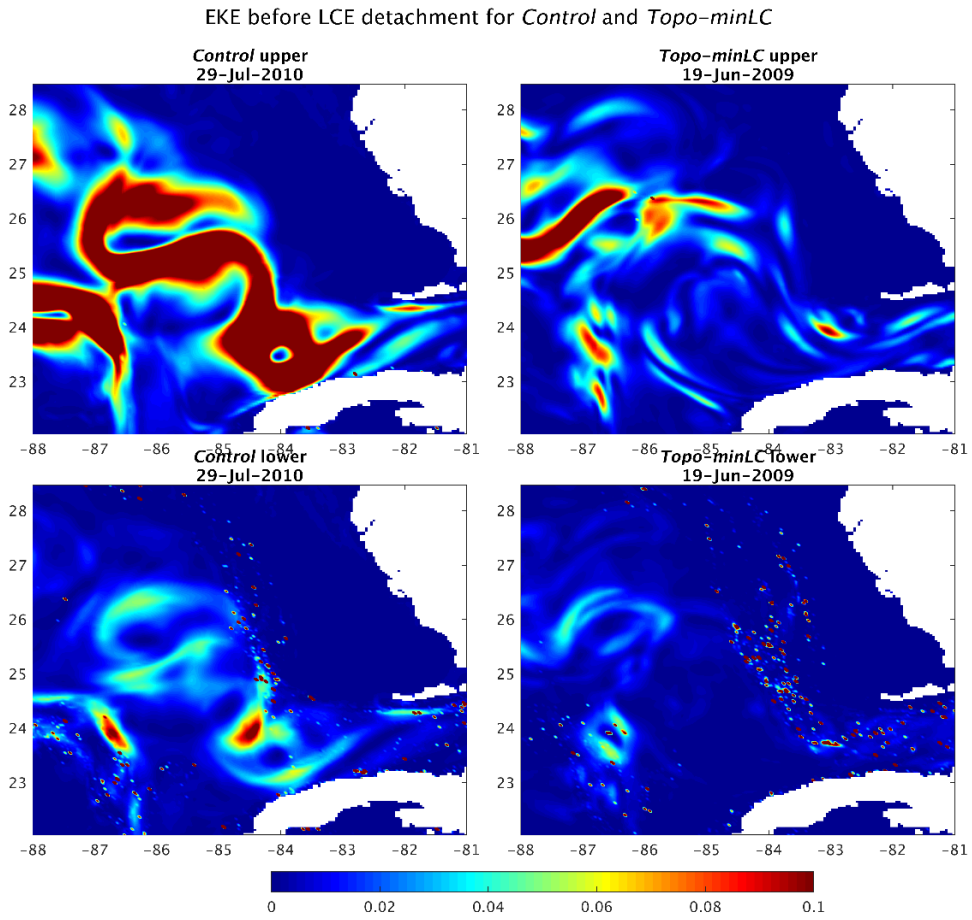

Figure 9: EKE calculated in a) Box 1 and b) Box 2 for the *Control* (solid blue line) and *Topo-minLC* (solid red line); see Figure 1 for Box locations. The vertical dashed blue and red lines represent final LCE separations in the *Control* and *Topo-minLC* experiments, respectively. c), e) EKE for the upper and lower layers of the *Control* before the LCE detachment, respectively, and d), f) EKE for the upper and lower layers of the *Topo-minLC* before the LCE detachment, respectively.

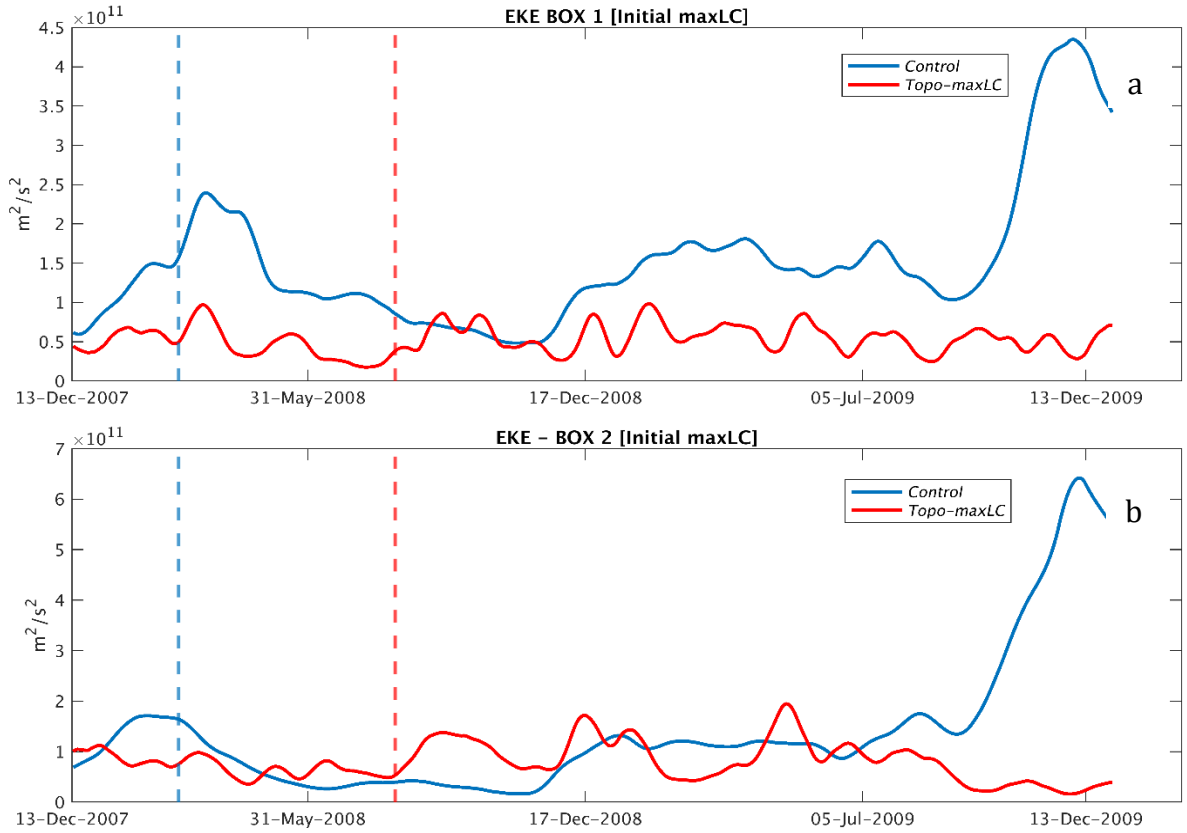

Figure 10: EKE calculated in a) Box 1 and b) Box 2 for the *Control* (solid blue line) and *Topo-maxLC* (solid red line); see Figure 1 for Box locations. The vertical dashed blue and red lines represent final LCE separations in the *Control* and *Topo-maxLC* experiments, respectively.

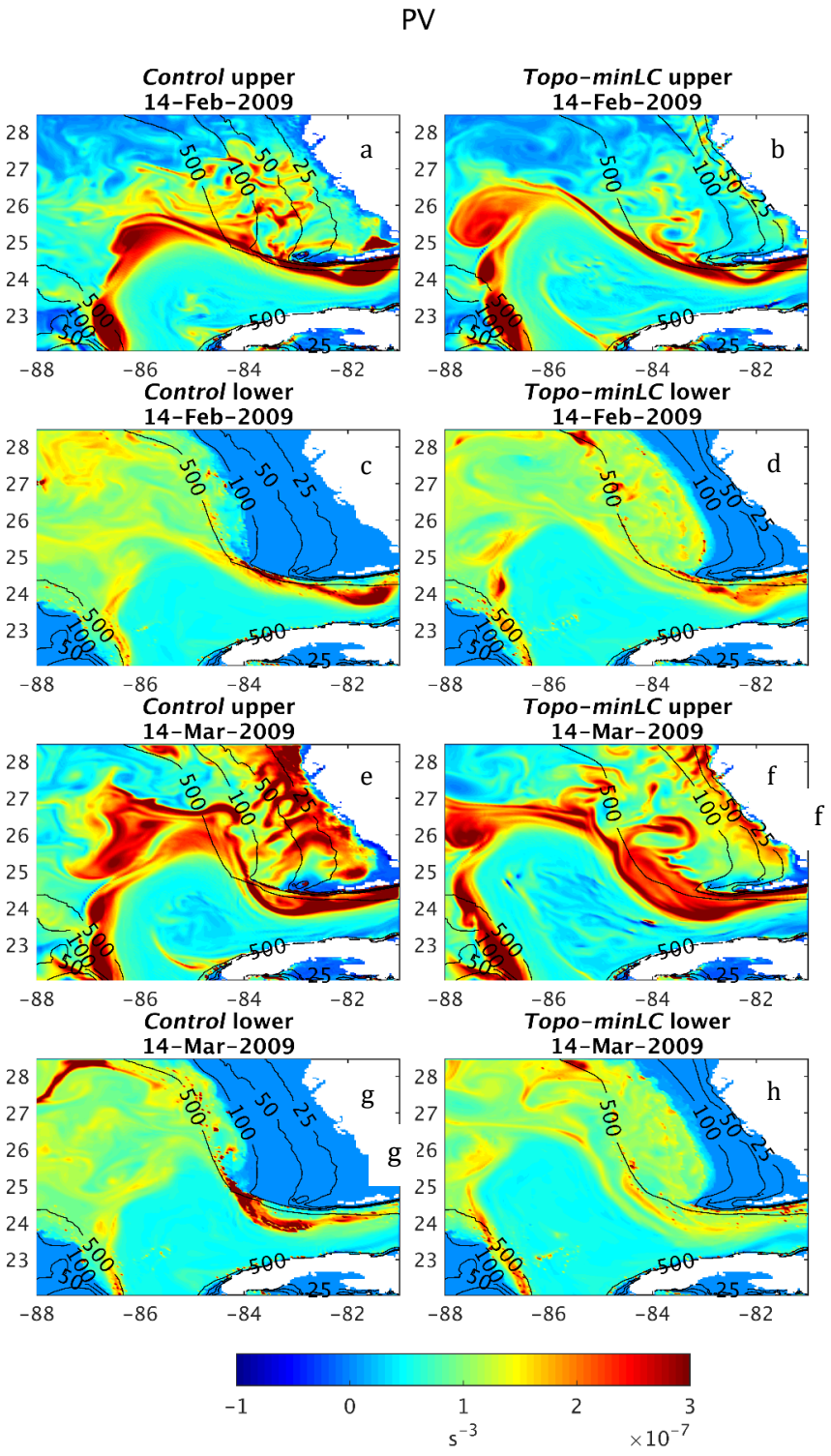

Figure 11: PV of the *Control* (left panels) and *Topo-minLC* (right panels) experiments, upper and lower layers, on February 14 (a-d) and March 14 (e-h), 2009. The black lines represent isobaths.

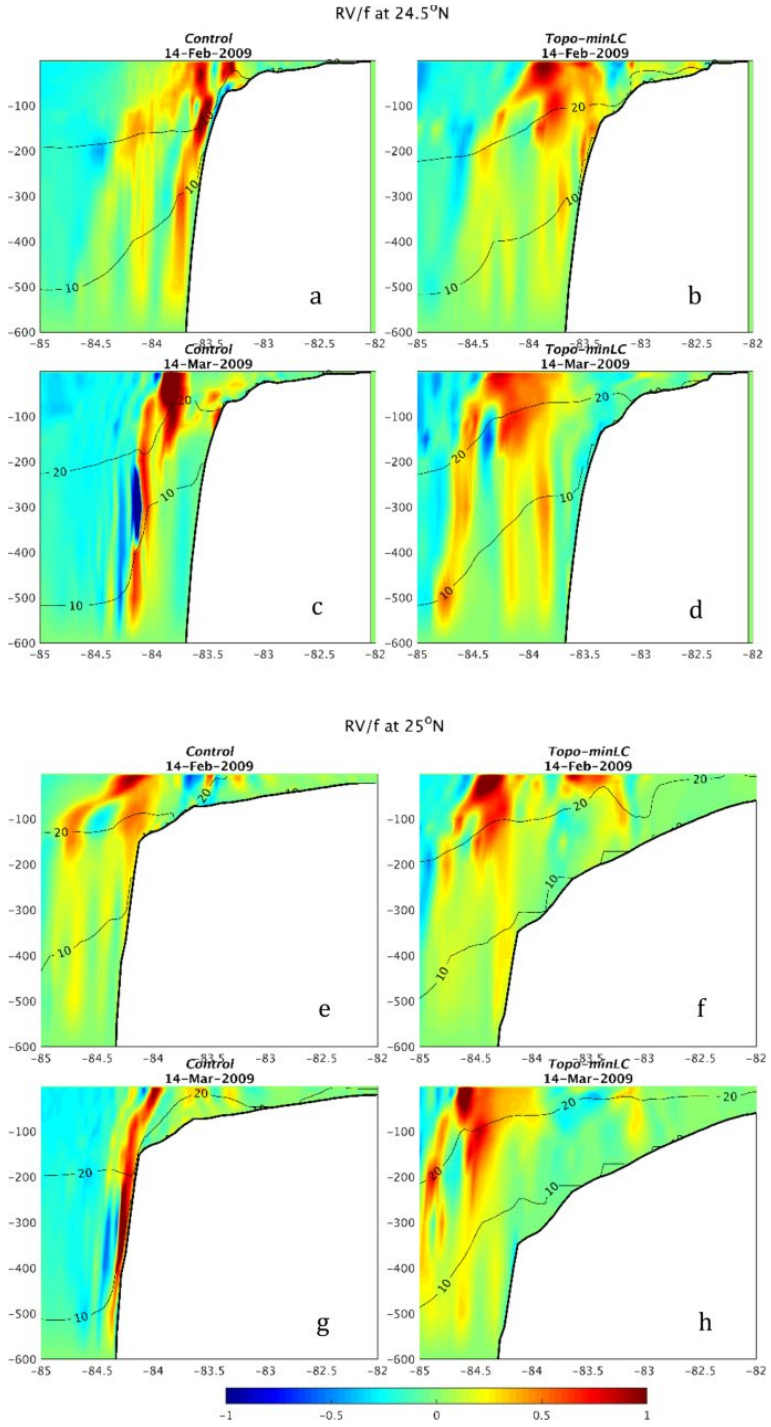

Figure 12: a)-d) Vertical sections of RV normalized by the Coriolis parameter f, at 24.5°N for the *Control* on a) February 14, 2009 and c) March 14, 2009 and for *Topo-minLC* on b) February 14, 2009 and d) March 14, 2009. e)-h) Vertical sections of RV/f at 25°N N for the *Control* on e) February 14, 2009 and g) March 14, 2009 and for *Topo-minLC* on f) February 14, 2009 and h) March 14, 2009. All panels represent the upper 600m of the water column. The black lines in each panel represent the 10°C and 20°C isotherms.

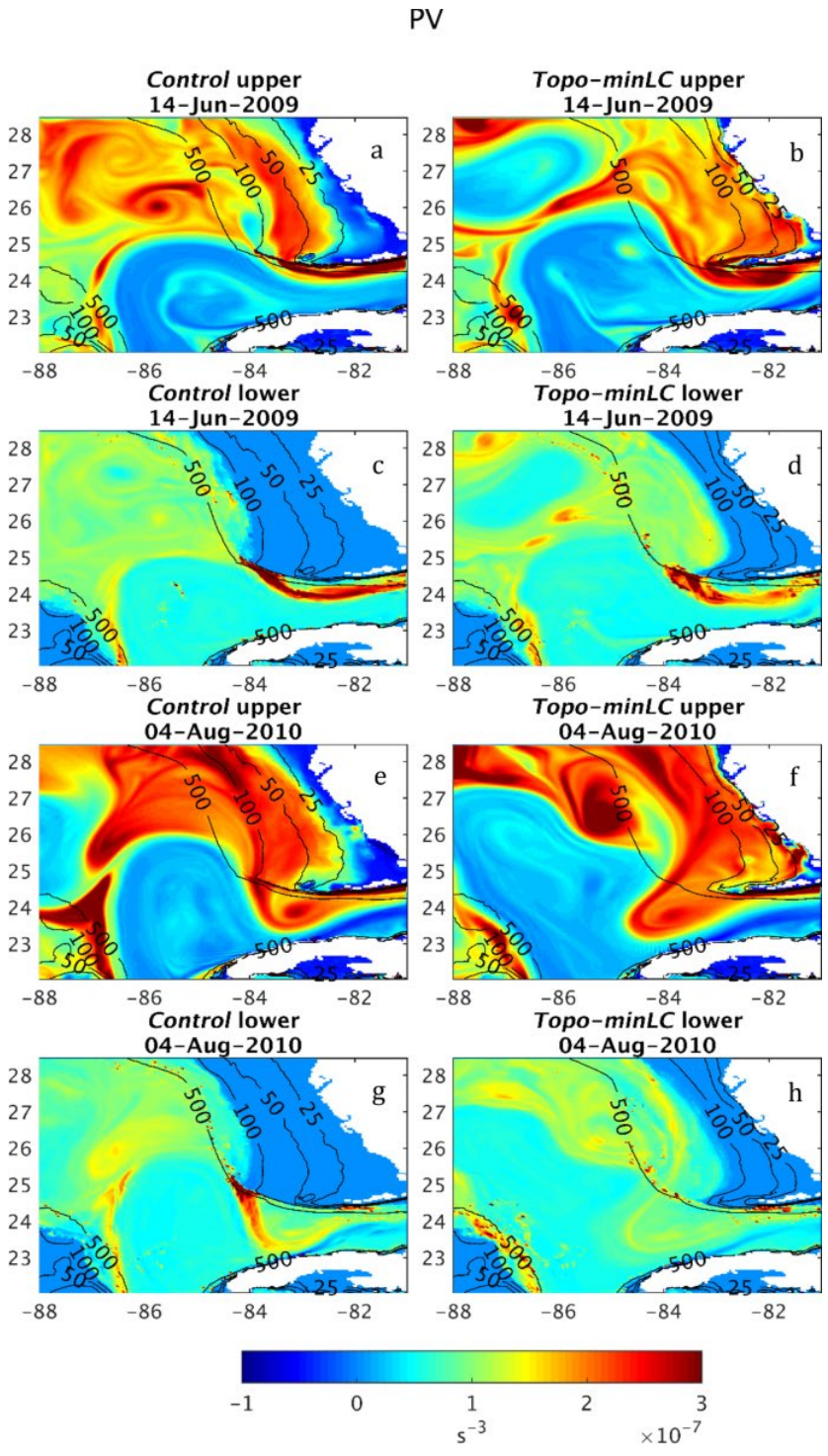

Figure 13: PV of the *Control* (leftel pans) and *Topo-minLC* (right panels) experiments, upper and lower layers, on June 14 (a-d), 2009 and August 4 (e-h), 2010. The black lines represent isobaths.

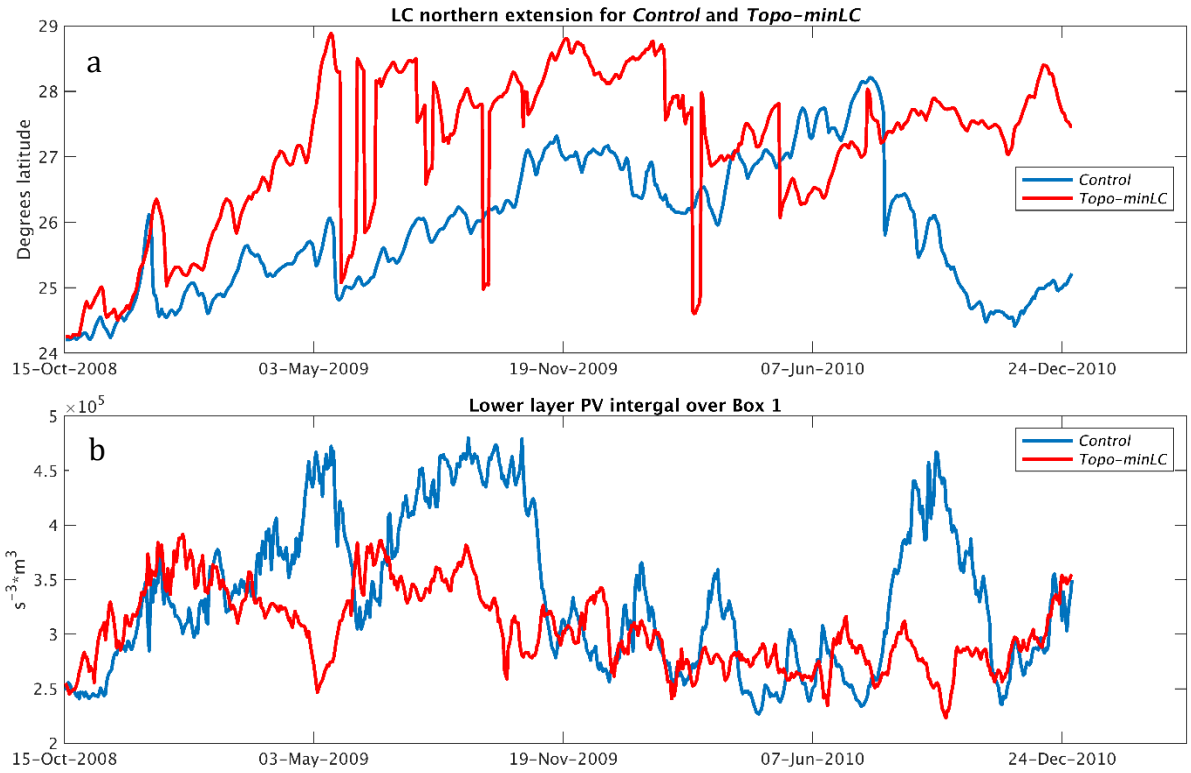

Figure 14: a) LC northernmost extension for *Control* (blue line) and *Topo-minLC* (red line) experiments. b) Integral of lower layer PV in Box 1 for *Control* (blue line) and *Topo-minLC* (red line) experiments; see Figure 1 for Box location.

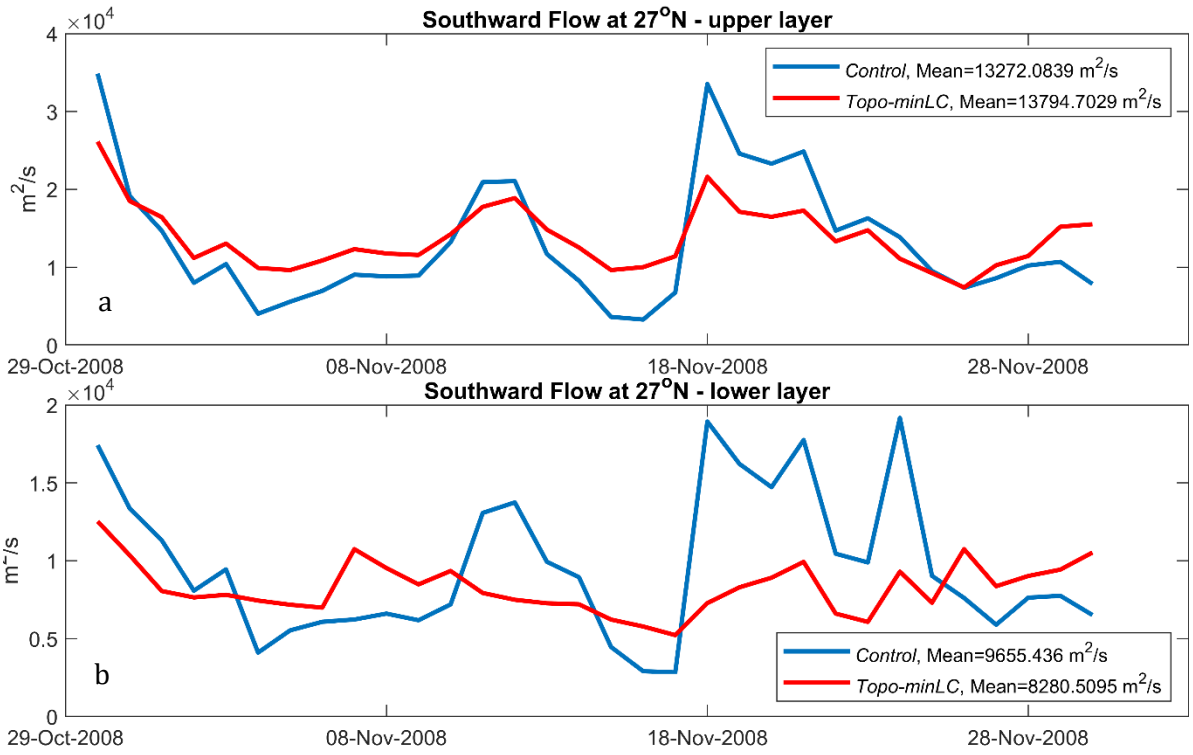

Figure 15: Absolute values of mean horizontally integrated southward currents at 27°N averaged over depth for the *Control* (blue lines) and *Topo-minLC* (red lines) experiments for the a) upper and b) lower layers.

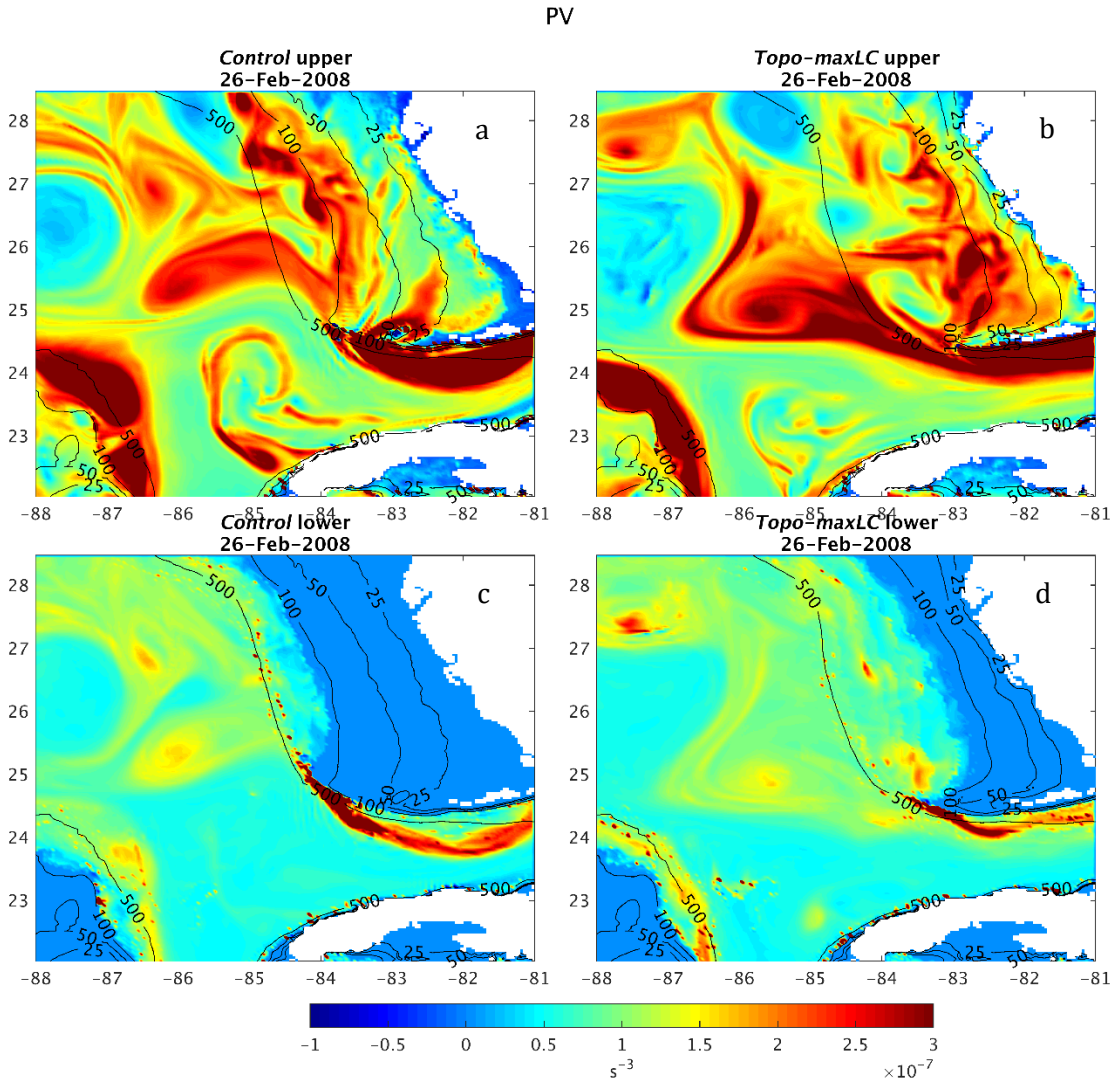

Figure 16: PV of the *Control* (left panels) and *Topo-maxLC* (right panels) on February 26, 2008, upper and lower layers. The black lines represent isobaths.

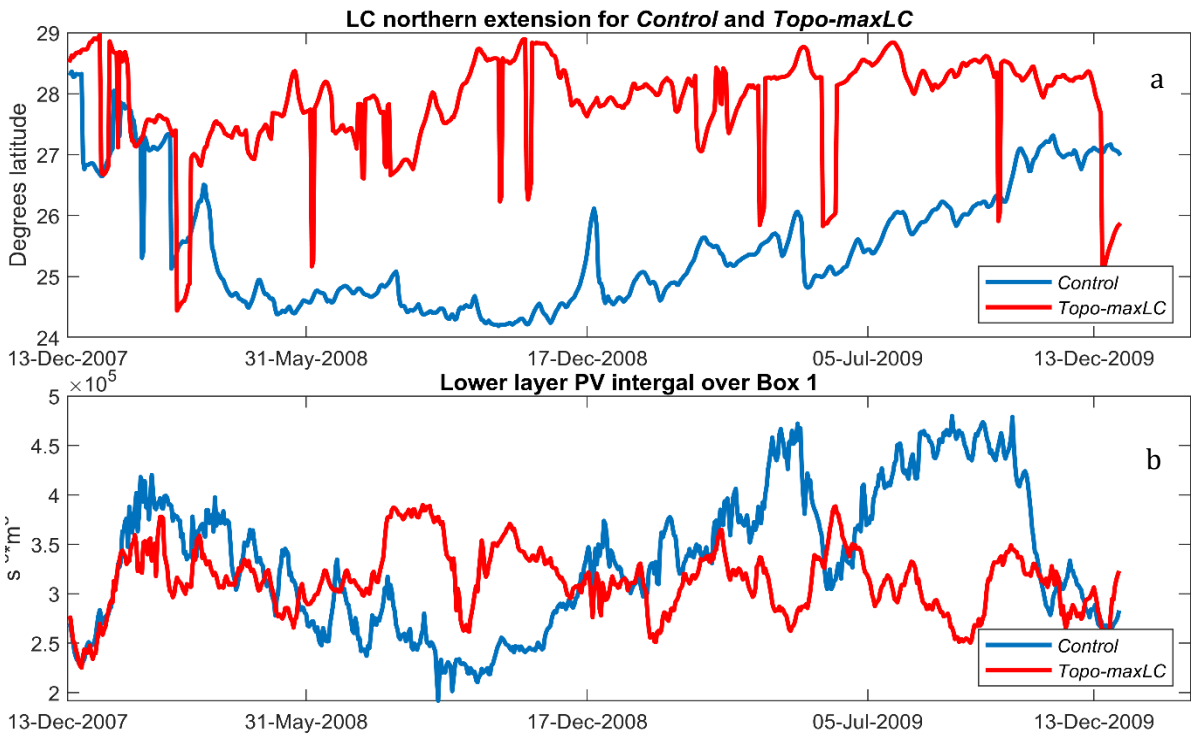

Figure 17: a) LC northernmost extension for *Control* (blue line) and *Topo-maxLC* (red line) experiments. b) Integral of lower layer PV in Box 1 for *Control* (blue line) and *Topo-maxLC* (red line) experiments; see Figure 1 for Box location.

Appendix: LC evolution in multi-year continuous simulations for realistic and modified WFS topographies

We performed a 5-year continuous simulation with the modified West Florida Shelf (WFS) topography ("*Modified"* experiment) to assess any long-term differences compared to the *Control* that were not evident in the 2-year simulations. The *Modified* experiment was initialized in May 2007, with the same initial conditions as the *Control.*

The LC northernmost extension for the 5-year period agrees with our findings from the 2-year simulations (Figures 4a and 4b), with the LC in the modified simulation mostly maintaining an extended phase with multiple LCE detachments/reattachments (abrupt drops in latitude) and a mean of 1 degree higher than the Control simulation (Figure A1).

Following the dynamical analysis based on the two-layer PV calculation presented in Section 4.2, the 5-year PV means of the *Control* and *Modified* experiments for the upper and lower layers are also in agreement with the results from the 2-year simulations (Figure A2). More specifically, on average, the LC in the *Modified* and *Topo-minLC* extends farther into the GoM compared to the *Control,* as shown in the mean upper layer PV (Figures A2a, A2c, and A2e), which supports the findings from Figure A1 and Figure 4a. The standard deviation of the upper layer PV showed higher variability of the LC position in the *Control* compared to the *Modified* (not shown), as expected from the LC northern extension presented in Figure A1. The mean upper layer PV in the southwestern WFS exhibits high positive values in both simulations, with the *Control* showing a slight intensification compared to the *Modified* and *Topo-minLC* (Figures A2a, A2c, and A2e). As mentioned in Section 4.2, the interaction between the LC system and the slope of the southwestern WFS in the *Control* leads to positive vorticity generation (Figure 12) that results in intensified lower layer PV in the region (i.e. Figures 11c and 11g). Such interaction is reduced in the *Topo-minLC* and *Topo-maxLC* experiments because of the deepening of the shelf slope (Figures 11d and 11h). This result is also supported by the 5-year continuous simulation, in which the mean lower layer positive PV in the southwestern

WFS is higher in the *Control* compared to the *Modified* experiment and the 2-year mean of the *Topo-minLC experiment* (Figures A2b, A2d, and A2f). In addition, the integrated lower layer PV over Box 1 in the *Modified* shows lower mean and especially lower variability, compared to the *Control* run (Figure A4a), also in agreement with the findings from the 2-year *Topo-minLC* and *Topo-maxLC* simulations (Figures 14b and 17b).

During retracted LC phases, another additional mechanism that can prevent the LC from extending northward and subsequently delay the LCE formation is the blocking from Loop Current Frontal Eddies (LCFEs) located north of the LC (Zavala-Hidalgo et al., 2006; Le Hénaff et al., 2014). We examined the surface cyclonic RV during two time periods of retracted LC phases in the *Control* and *Modified* experiments to further investigate the blocking effects of LCFEs in the two experiments. The surface cyclonic RV was spatially averaged over a box region (24°N-28°N, 88°W-84°W) when the LC was retracted. The results show no significant differences in the signature of the LCFEs north of the retracted LC between the two experiments, indicating that the LCFE blocking is not responsible for the differences in the LC behavior between the *Control* and *Modified* experiments (Figure A3).

Focusing on the periods of extended LC in the *Control* and *Modified* simulations, we expect the generation of lower-layer positive PV to be less pronounced than when the LC is retracted. As previously shown in Weisberg and Liu (2017), when this LC is extended, it generally moves away from the southwestern tip of the WFS. Figures A4b-A4e show the mean upper- and lower-layer PV of the *Control* and *Modified* experiments only for the days in the 5-year simulation when the northern extension of the LC is north of 27.5°N, representing extended LC phases. The LC is the *Control* spends a total of 192 days in an extended phase (north of 27.5°N), whereas in the *Modified*, the total number of days of extended LC phases is 622, supporting our hypothesis that the interaction with the shelf can play a role to the LC northern extension. Focusing on the lower layer, (Figures A4d and A4e), although the levels of positive PV on the southwestern WFS are comparable, the length of the segment of high PV is larger in the *Control* experiment as it extends further to the northwest than in the

Modified experiment (Figure A4d). This is directly related to the shape of the WFS in the *Modified* experiment, in which the shelf area is reduced, and the shallow isobaths are pushed eastward toward the coast along most of the WFS, compared to the *Control* experiment. As a result, the interaction between the LC and the upper continental shelf break is confined to a smaller area where the isobaths are wrapping around the southwestern tip of the WFS (Figure A4e). The interaction between the LC and the southwest Florida Shelf, identified through positive PV generation, thus differs between the modified topography and the *Control* experiments not only on average or when the LC is retracted, but also when the LC is extended. The differences are not as pronounced, because the level of interactions between the LC and the southwest Florida Shelf is expected to be lower when the LC is extended compared to when it is retracted.

Overall, the results from the 5-year continuous simulations support the shorter-term runs (*Topo-minLC* and *Topo-maxLC*) and show that the case-oriented processes that were presented in Sections 3.2 and 4.2 also correspond to a general behavior of the LC system when interacting with the topography of the southwestern WFS.

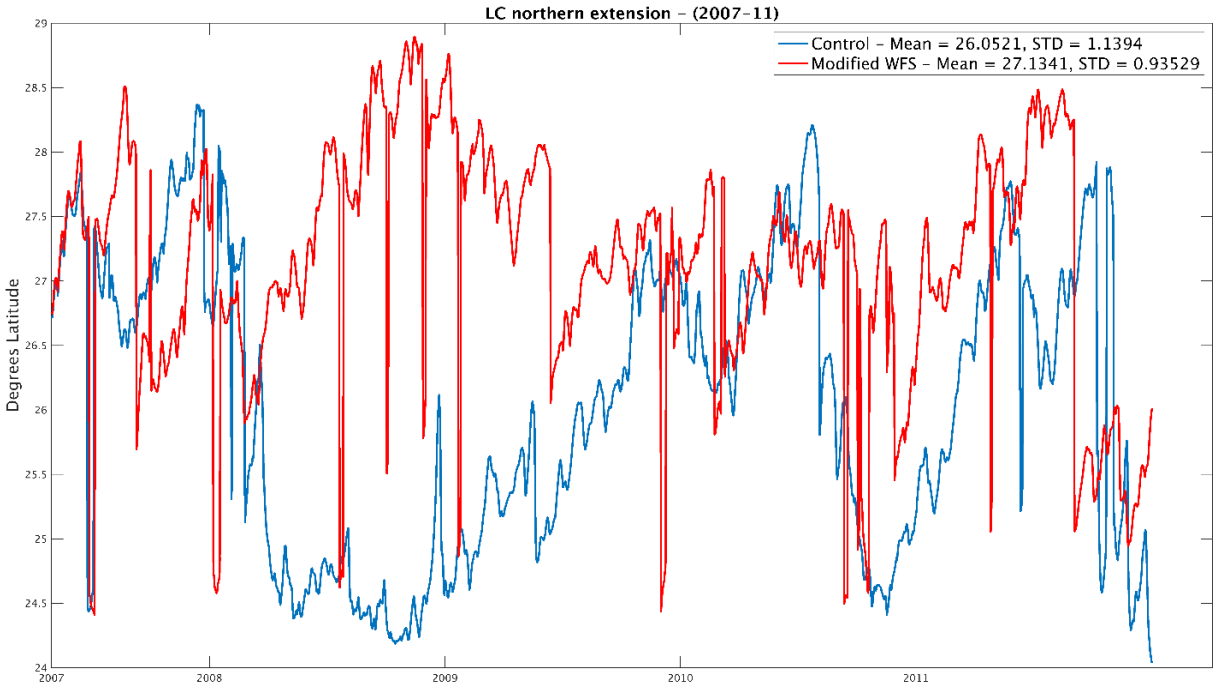

Figure A1: LC northern extension for two continuous 5-year simulations for the Control (blue line) and Modified (red line) experiments. Both simulations were initialized at the same state, in May 2007.

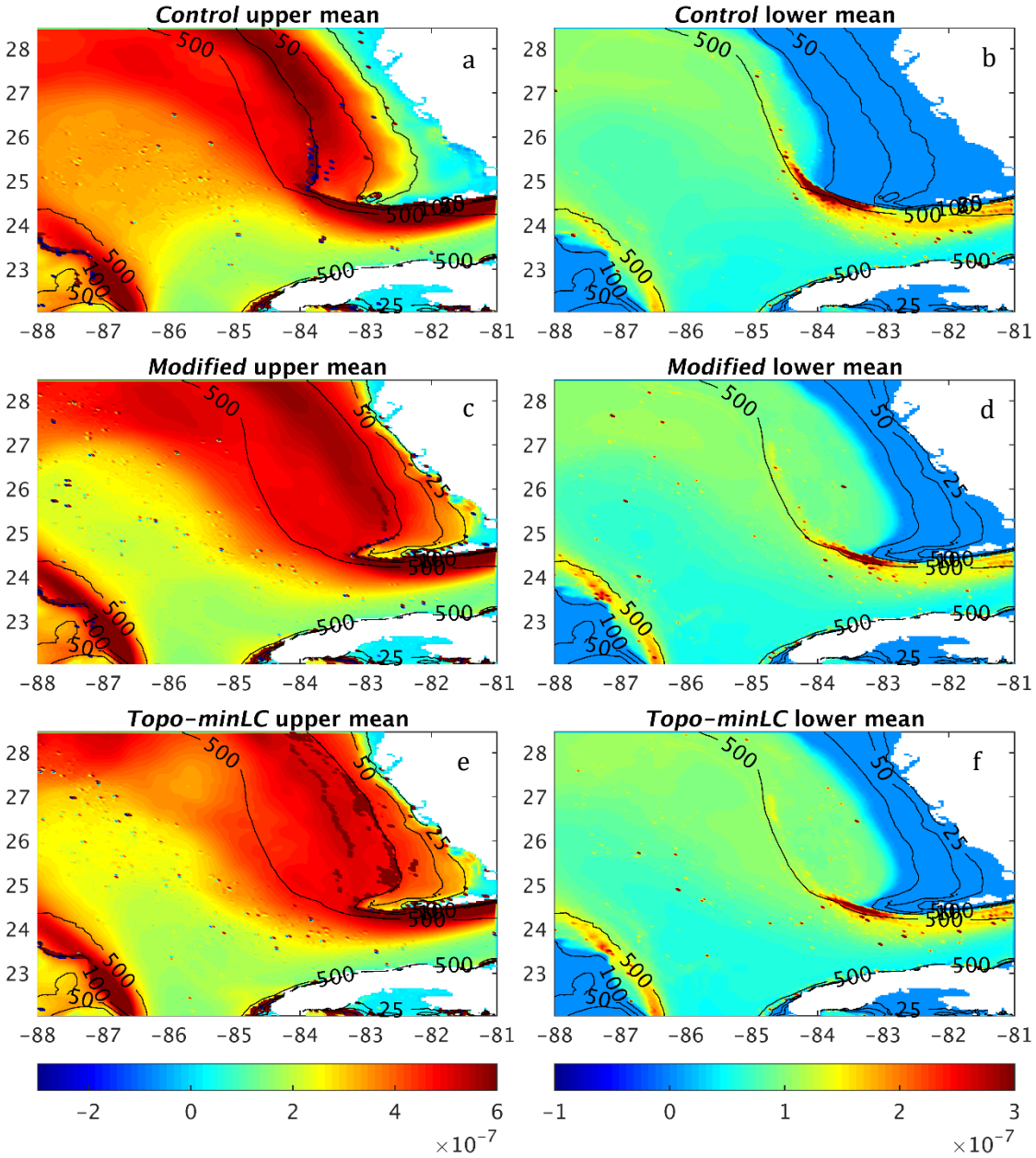

Figure A2: Temporal mean of the 5-year continuous simulation (2007-2011) for a)-b) the *Control* and c)-d) *Modified* experiments and e)-f) of the 2-year *Topo-minLC,* upper and lower layers. The black lines represent isobaths. The color scales for the upper and lower layers are different for clarity.

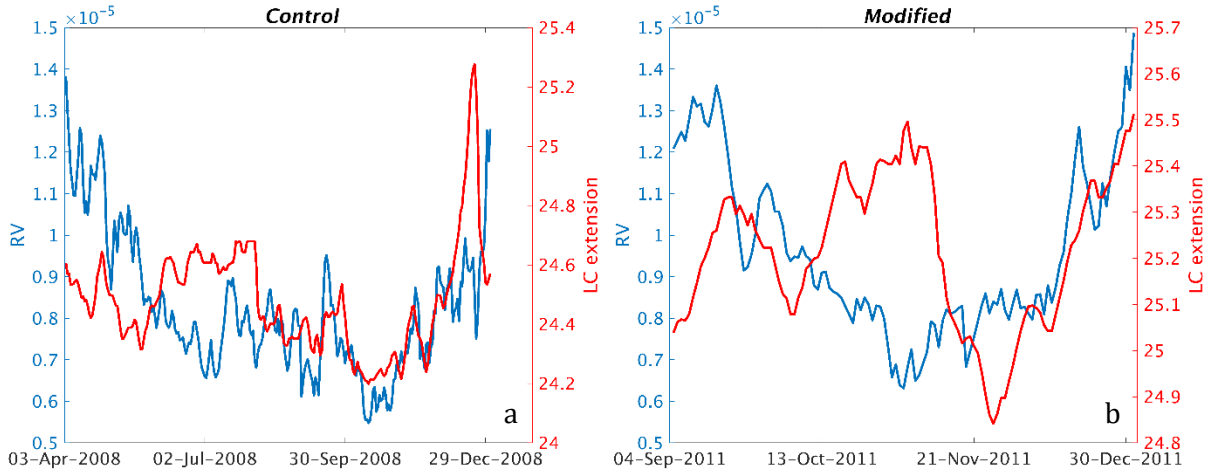

Figure A3: Surface relative vorticity spatially averaged over a box region (24°N-28°N, 88°W-84°W) (blue) and LC northern extension (red) for the a) *Control* and b) *Modified* experiments for retracted LC phases, with northern LC extensions south of than 25.5°N (273 days in Control and 119 days in the Modified).

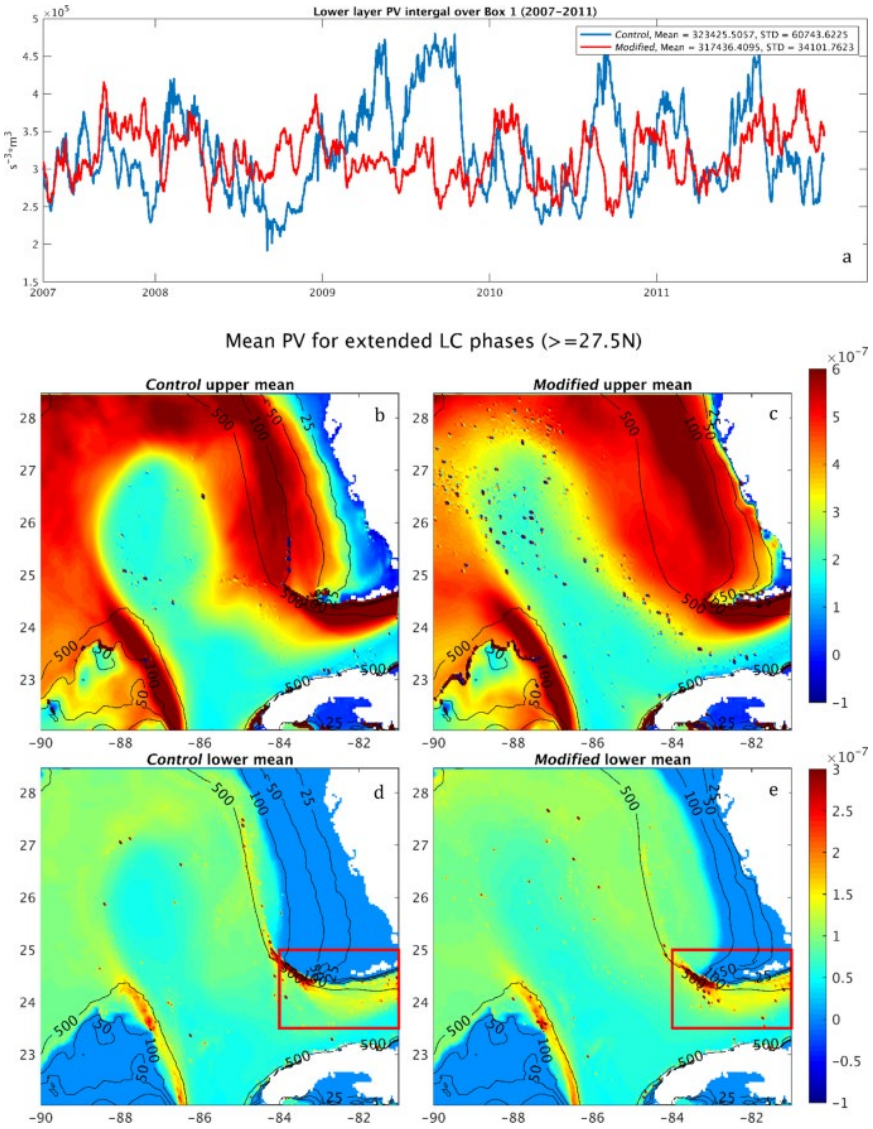

Figure A4: a) Integrated lower layer PV in Box 1 (shown in panels d) and e)) for *Control* (blue line) and *Modified* (red line) experiments, from 2007 to 2011, b) and c) Mean PV of upper layer for the Control Modified experiments, respectively, for extended LC phases, with northern LC extensions larger than 27.5°N (192 days in *Control* and 622 days in the *Modified*), d) and e) same as b) and c) but for the lower layer. The red box in indicates the location of Box 1.